Heat Transfer and Pressure Drop Characteristics of R-22, R-134A and R-407C in Microchannel Tubes

A. Vardhan and W. E. Dunn

ACRC TR-133 November 1997

For additional information:

Air Conditioning and Refrigeration Center
University of Illinois
Mechanical & Industrial Engineering Dept.
1206 West Green Street
Urbana, IL 61801

(217) 333-3115

Prepared as part of ACRC Project 75
Microchannel Heat Exchangers
W. E. Dunn, Principal Investigator

The Air Conditioning and Refrigeration Center was founded in 1988 with a grant from the estate of Richard W. Kritzer, the founder of Peerless of America Inc. A State of Illinois Technology Challenge Grant helped build the laboratory facilities. The ACRC receives continuing support from the Richard W. Kritzer Endowment and the National Science Foundation. The following organizations have also become sponsors of the Center.

Amana Refrigeration, Inc.
Brazeway, Inc.
Carrier Corporation
Caterpillar, Inc.
Copeland Corporation
Dayton Thermal Products
Delphi Harrison Thermal Systems
Eaton Corporation
Ford Motor Company
Frigidaire Company
General Electric Company
Hydro Aluminum Adrian, Inc.
Indiana Tube Corporation
Lennox International, Inc.
Modine Manufacturing Co.
Peerless of America, Inc.
Redwood Microsystems, Inc.
The Trane Company
Whirlpool Corporation
York International, Inc.

For additional information:

Air Conditioning & Refrigeration Center
Mechanical & Industrial Engineering Dept.
University of Illinois
1206 West Green Street
Urbana IL 61801

217 333 3115

Abstract

A study of heat transfer and pressure drop characteristics for single-phase and two-phase flow of refrigerants in microchannel tubes was conducted. An existing facility was modified to perform tests on a single microchannel tube using water flowing in counterflow as the heat sink fluid. Data were collected for subcooled liquid, superheated vapor and condensing refrigerant for circular-port microchannel tubes at four different mass flow rates. The refrigerants tested were R-22, R-134a and R-407C. In addition to circular-port tubes, square-port tubes were tested with R-22 for both single-phase and two-phase flow. Data were also taken with water flowing inside a square-port microchannel tube. The Reynolds number for all the flows in this study ranged from 3,000 to 17,000 in the liquid phase and 30,000 to 110,000 in the vapor phase.

The heat transfer coefficients and pressure drop for circular-port microchannel tubes were compared for R-22, R-134a and R-407C. For subcooled liquid flow, the heat transfer coefficient for R-407C was found to be greater than that for R-22 and R-134a. The heat transfer coefficient for R-22 was found to slightly lesser than the other two refrigerants for condensing flow.

A model was built to predict the heat transfer and pressure drop in the microchannel tube. In most cases, the heat transfer and pressure drop predicted by the model agree very well with experimental results. A sensitivity analysis revealed that the total heat transfer is not very sensitive to the refrigerant side heat transfer coefficient.

Table of Contents

List of Tables

List of Figures

Nomenclature

English symbols

A	free-flow area
D	tube diameter
D_h	hydraulic diameter
F_{tp}	two-phase multiplier
f_C	Churchill friction factor
f_D	Darcy friction factor
f_F	Fanno friction factor
G	mass flux
h	fluid enthalpy
$\dot{m}$	mass flow rate
Nu	Nusselt number
p	fluid pressure
Pr	Prandtl number
Pr_w	Prandtl number based on properties at the wall temperature
P_{red}	reduced pressure
Re	Reynolds number
T	fluid temperature
UA	heat transfer coefficient times heat transfer area
X	Lohkhart Martinelli parameter

$X_{tt,q}$	Modified Lohkhart Martinelli parameter for heat transfer (defined Equation 2.55)
x	quality

Greek symbols

ϵ	effective surface roughness
μ	fluid viscosity
ϕ	Multiplier used by Lockhart and Martinelli
ρ	fluid density
τ_w	perimeter-average wall shear stress

Superscripts

old	property values from previous iteration

Subscripts

inside	pertaining to inside surface of tube
l	assumes actual liquid flow rate occupies entire tube, *eg* $Re_l = \frac{GD(1-x)}{\mu_l}$
lo	assumes all flow is liquid and occupies entire tube, *eg* $Re_{lo} = \frac{GD}{\mu_l}$
outside	pertaining to outside surface of tube
v	assumes actual vapor flow rate occupies entire tube, *eg* $Re_v = \frac{GD(1-x)}{\mu_v}$
vo	assumes all flow is vapor and occupies entire tube,*eg* $Re_{vo} = \frac{GD}{\mu_v}$

Chapter 1

Introduction

Microchannel heat exchanger technology is a relatively new technology made possible by advances in aluminium extrusion and brazing proceses. It is used extensively for the construction of compact condensers used in mobile air-conditioning units. Microchannel condensers provide several advantages over conventional condensers but information about their heat transfer and pressure drop characteristics is still not very extensive.

The present study documents the results obtained from heat transfer and pressure drop experiments on microchannel tubes.

1.1 Microchannel Heat Exchanger Description

Figure 1.1 shows a typical microchannel condenser. The distinguishing feature of microchannel heat exchangers is that they are made of flat aluminium tubes (called microchannel tubes) each having a number of small ports with hydraulic diameter on the order of 1 mm. As shown in the figure, the tubes are arranged horizontally with air-side louvered fins separating them. The ends of the tubes are brazed to large diameter headers which also serve to provide mechanical rigidity to the whole assembly. The refrigerant is circuited by baffles inside the headers. A number of different port geometries for the microchannel tube are popular, some of them being shown in Figure 1.2.

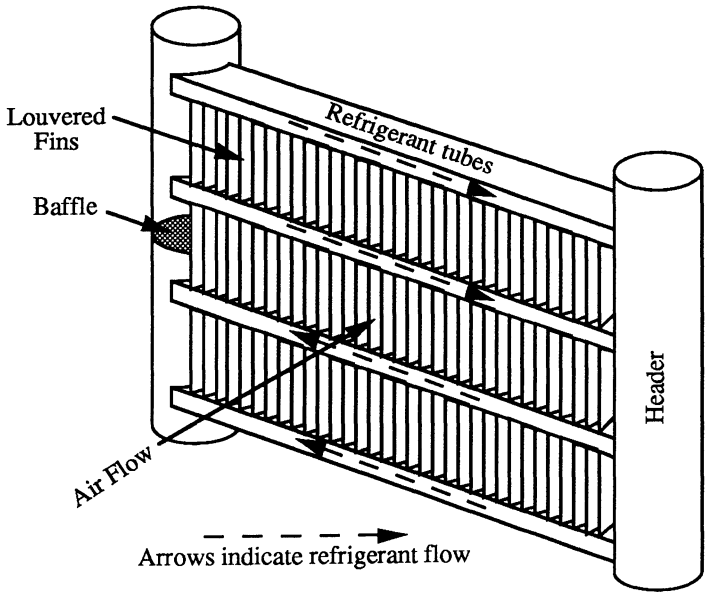

Figure 1.1: A microchannel heat exchanger.

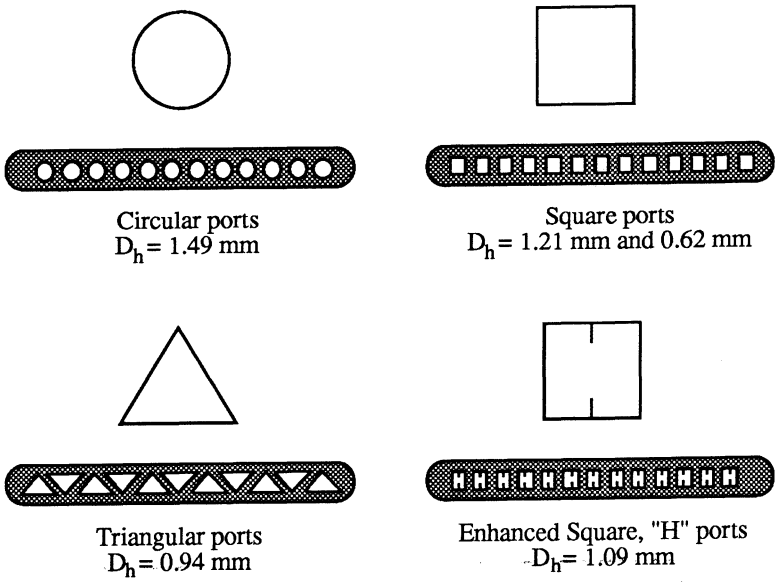

Figure 1.2: Microchannel port shapes.

Another notable feature of microchannel heat exchangers is the low-cost flexibility of refrigerant circuiting afforded by the headers, baffles and refrigerant tubes. They also offer improved thermal performance and compact designs with lower requirements for refrigerant charge. This has made the technology popular for mobile air-conditioning condensers. Use of this technology for condensers in stationary applications and for evaporators is also being evaluated.

1.2 Objectives

The objectives of this study are to quantify the heat transfer and pressure drop characteristics of microchanel tubes for both single-phase and two-phase condensing flow. Three different refrigerants, namely, R-22, R-134a and R-407c are tested.

The test facility for this study uses a single microchannel tube which flows refrigerant in counterflow to water. The details of the facility are described later.

Chapter 2

Literature Review

2.1 Introduction

This chapter reviews many references relevant to the present work. Results for both single-phase and two-phase heat transfer and pressure drop are described. Finally, other microchannel tube heat transfer and pressure drop studies are discussed.

2.2 Single-phase Pressure drop

Much of the literature dealing with frictional pressure drop and heat transfer is concerned with tube diameters greater than 20 mm, whereas this study considers tubes with hyadraulic diameter on the order of 1 mm. The correlations for pressure drop are usually expressed in terms of friction factors. Several definitions of the friction factor are found in the literature, including the Darcy friction factor:

$$f_D = \frac{4\tau_w}{\frac{1}{2}\rho V^2}, \tag{2.1}$$

where τ_w is the perimeter-average wall shear stress, ρ is the fluid density and V is the fluid velocity.

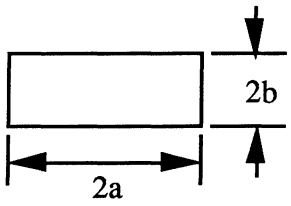

Figure 2.1: Rectangular duct geometry

The Darcy friction factor f_D is related to the Fanning f_F and Churchill f_C friction factors by

$$f_C = f_F/2 = f_D/8 \tag{2.2}$$

In the fully developed region of the duct, the velocity profile is invariant at any flow cross section. The momentum balance in this region has the following form:

$$\frac{\Delta p}{\frac{1}{2}\rho V^2} = f_D \frac{\Delta x}{D_h}, \tag{2.3}$$

where Δp is the incremental pressure drop, Δx is the incremental length and D_h is the hydraulic diameter of the duct. Length scales other than the hydraulic diameter may also be used.

2.2.1 Pressure Drop in fully developed laminar flow

The friction factor for fully developed laminar flow can be found analytically by solving the axial momentum equation. For circular ducts this can be shown to be (See Incropera and Dewitt (1990)),

$$f_F = \frac{64}{Re} \tag{2.4}$$

However, friction factor relations in noncircular ducts are not as simple. We define the geometry of rectangular and triangular ducts by Figures 2.1 and 2.2.

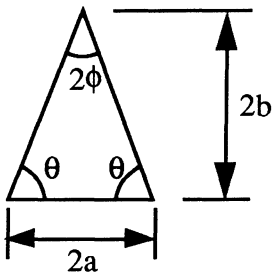

Figure 2.2: Triangular duct geometry

Shah and London (1978) present the folowing relation for the laminar friction factor for flow in a rectangular duct.

$$f_F Re_h = 24(1 - 1.3553\alpha^* + 1.9467\alpha^{*2} - 1.7012\alpha^{*3} + 0.9564\alpha^{*4} - 0.2537\alpha^{*5}), \quad (2.5)$$

where

$$\alpha^* \equiv \frac{2b}{2a}. \quad (2.6)$$

Equation 2.5 is derived from an approximation to an infinite series solution for the fully developed velocity profile in a rectangular duct. For square ducts ($\alpha^* = 1$) we get $f_F Re_h = 14.22708$.

Shah and London (1978) provide the following correleation for the laminar friction factor in triangular ducts.

$$f_F Re_h = \frac{12(B+2)(1-\tan^2\phi)}{(B-2)\left[\tan\phi + (1+\tan^2\phi)^{\frac{1}{2}}\right]^2}, \quad (2.7)$$

where

$$B = \left[4 + \frac{5}{2}\left(\frac{1}{\tan^2\phi} - 1\right)\right]^{1/2}. \quad (2.8)$$

For equilateral triangular ducts ($\phi = 30°$) one obtaines $f_F Re_h = 13.33$.

2.2.2 Fully developed turbulent pressure drop

The prediction of friction factors for turbulent single-phase flow is considerably more difficult than that for laminar single-phase flow.

Many friction factor correlations have been developed for Gerhart and Gross (1985) tubulent-flow pressure drop in circular pipes. present a history of the development of friction factor correlations. In 1935, Prandtl developed the following formula for turbulent flow in smooth pipes.

$$\frac{1}{\sqrt{4f_F}} = 2.0\log(Re\sqrt{4f_F}) - 0.8 \tag{2.9}$$

Here, "smooth" means that the wall roughness elements are assumed to be so small that their influence does not extend beyond the laminar sublayer.

Around the same time, von Karman presented the following relation for turbulent flow in fully rough circular pipe flow.

$$\frac{1}{\sqrt{4f_F}} = -2.0\log(\frac{\epsilon/D}{3.7}) \tag{2.10}$$

"Fully rough" turbulent flows is supposed to occur when the roughness elements extend throught the turbulent boundary layer into the turbulent core of the flow. In this case, as Reynolds number increases, the boundary layer becomes thinner. Because the boundary layer is fully disrupted by the roughness elements, increased Reynolds number does not affect the friction factor.

In 1939, Colebrook developed a formula that accounted for the smooth and fully rough regions as well as the transituon zone between.

$$\frac{1}{\sqrt{4f_F}} = -2.0\log(\frac{2.51}{Re\sqrt{4f_F}} + \frac{\epsilon/D}{3.7}) \tag{2.11}$$

Churchill (1977) devloped an explicit asymptotic representation for turbulent friction factor for both laminar and turbulent regions (including both smooth and fully rough

pipes):

$$f_C = \left[\left(\frac{8}{Re}\right)^{12} + \frac{1}{(A+B)^{3/2}}\right]^{1/12}, \tag{2.12}$$

where

$$A = \left[2.457 \ln\left(\frac{1}{(7/Re)^{0.9} + 0.27\epsilon/D}\right)\right]^{16} \tag{2.13}$$

and

$$B = \left(\frac{37,530}{Re}\right)^{16}. \tag{2.14}$$

We use a slightly modified form of the asymptotic representation

$$f_D = \left[\left(\frac{64}{Re}\right)^{12} + \frac{1}{(A+B)^{3/2}}\right]^{1/12}, \tag{2.15}$$

where

$$A = \left[0.86868 \ln\left(\frac{1}{(7/Re)^{0.9} + 0.27\epsilon/D}\right)\right]^{16} \tag{2.16}$$

and

$$B = \left(\frac{12,990}{Re}\right)^{16}. \tag{2.17}$$

2.2.2.1 Moody chart

To facilitate engineering calculations, Moody (1944) developed the classical presentation of circular duct friction pressure drop data in which f_D is plotted against Re based on previously accepted conclusions.

2.2.2.2 Noncircular ducts

Although unique *laminar* friction factor correlations must be used for each tube geometry, Bhatti and Shah (1987) indicate that *turbulent* friction factors may be scaled to match the circular duct results by using an *effective diameter* as the length scale for the Reynolds number. Obot (1988) argues that complete dynamic similarity between circular ducts and noncircular ducts can be obtained if *both* the Reynolds number and friction factor are appropriately scaled. Appropriate scaling produces similarity in the *critical values* of both Reynolds number and the friction factor. Obot notes that the use of hydraulic diameter for reducing experimental pressure drop daa is advantageous as it brings the value of the critical friction factor for any duct geometry in agreement with that for a circular tube. The remaining task is to identify a scale to be used for Reynolds number that equates the critical value of Reynolds number for all geometries with the critical Reynolds number for circular ducts. Different approaches to finding this *effective diameter* can be seen in Mikic et al. (1994), Jones (1976), Obot (1988) and Bhatti and Shah (1987).

2.3 Single-phase Heat transfer

2.3.1 Fully developed laminar flow

Typically, for fully developed laminar flow, the Nusselt number, defined as:

$$Nu \equiv \frac{hD}{k}, \tag{2.18}$$

is presented independent of Re and Pr which is correct to the first order of approximation. For constant wall temperature, Nu is 3.657 for circular ducts, 2.47 for equilateral triangular ducts and 2.976 for square ducts. Shah and London (1978) have compiled the information for various other geometries.

2.3.2 Fully developed turbulent flow

The classical correlation for fully developed turbulent flow is the Dittus-Boelter equation:

$$Nu = 0.023 Re^{4/5} Pr^{n}, \tag{2.19}$$

where $n = 0.4$ for fluid heating (wall hotter than fluid), and $n = 0.3$ for fluid cooling (wall colder than fluid).

Gnielinski (1976) utilized a comprehensive set of experimental data from a variety of studies to develop the following correlation.

$$Nu = \frac{(4f_F/8)\,(Re - 1000)Pr}{1 + 12.7\sqrt{4f_F/8}(Pr^{2/3} - 1)} \left[1 + (D/L)^{2/3}\right] \frac{Pr}{Pr_w}^{0.11} \tag{2.20}$$

The Gnielinski correlation requires

$$4f_F = [1.82 \ln(Re) - 1.64]^{-2} \tag{2.21}$$

for $Re > 10^4$, and

$$4f_F = 0.3164 Re^{-1/4} \tag{2.22}$$

for $2300 \leq Re \leq 10^4$

Although Gnielinski's correlation is purported to be accurate for $Re \geq 2300$, Heun (1995) has expressed reservations about the correllation for data with $Re < 5000$.

2.4 Two-phase Pressure Drop

2.4.1 Lockhart and Martinelli's correlation

Lockhart and Martinelli (1949) published the seminal work on two-phase flow frictional pressure drop. The liquid and the vapor phases can be turbulent or laminar leading to

four combinations of flows. Lockhart and Martinelli assumed that the two-phase frictional pressure drop can be expressed by any of the following equations:

$$\left(\frac{dP}{dz}\right) = {\phi_l}^2\left(\frac{dP}{dz}\right)_l, \tag{2.23}$$

$$\left(\frac{dP}{dz}\right) = {\phi_{lo}}^2\left(\frac{dP}{dz}\right)_{lo}, \tag{2.24}$$

$$\left(\frac{dP}{dz}\right) = {\phi_v}^2\left(\frac{dP}{dz}\right)_v, \tag{2.25}$$

$$\left(\frac{dP}{dz}\right) = {\phi_{vo}}^2\left(\frac{dP}{dz}\right)_{vo}. \tag{2.26}$$

The single-phase pressure drops are given by

$$-\frac{dP}{dz} = 2\frac{f_F G^2}{\rho D}, \tag{2.27}$$

where mass flux G is based on the appropriate velocity V_l, V_{lo}, V_v or V_{vo}. Lockhart and Martinelli proposed that any of the two-phase multipliers ϕ^2 should be a function of the ratio of the liquid and vapor frictional pressure drop predictions. This parameter, now known as the Lokhart-Martinelli parameter, is given by

$$X^2 = \frac{\left(\frac{dP}{dz}\right)_l}{\left(\frac{dP}{dz}\right)_v} = \frac{2\frac{a_l}{{Re_l}^{n_l}}\frac{G^2(1-x)^2}{\rho_l D}}{2\frac{a_v}{{Re_v}^{n_v}}\frac{G^2(1-x)^2}{\rho_v D}} = \frac{a_l}{a_v}\frac{{\mu_l}^{n_l}}{{\mu_v}^{n_v}}\frac{\rho_v}{\rho_l}\frac{(1-x)^{(2-n_l)}}{x^{(2-n_v)}} \tag{2.28}$$

The coefficients a_l, a_v, n_l and n_v depend on the nature of the liquid or vapor flow in each phase.

The final remaining task is to find the relationship between ϕ and X. Experimental data are used to quantify the relationship. Lockhart and Martinelli present the data graphically, but Chisholm and Laird (1958) performed a curve fit with functions of the form

$${\phi_l}^2 = 1 + \frac{C}{X} + \frac{1}{X^2}, \tag{2.29}$$

Liquid Flow	Vapor Flow	C
Turbulent	Turbulent	20
Laminar	Turbulent	12
Turbulent	Laminar	10
Laminar	Laminar	5

Table 2.1: Constants for two-phase multiplier correlation

and

$$\phi_v{}^2 = 1 + CX + X^2. \tag{2.30}$$

The value for the various constants are given in Table 2.1.

2.5 Condensation Heat Transfer

Condensation heat transfer and more generally two-phase heat transfer have been studied extensively by many researchers. Two-phase flow can be broadly classified into three categories: (a) gravity-controlled flows, (b) vapor-shear controlled flows, and (c) intermittent flows. The heat transfer correlations obviously depend on the flow regime. In our experiments with microchannel tubes, the mass flux of the refrigerant flowing inside the tube is always greater than $430\frac{kg}{m^2 s}$ and we assume that in all cases we have vapor-shear controlled annular flow. We shall now describe some of the correlations applicable to our case.

2.5.1 Two-phase multiplier-based correlations

The basic premise for this approach is that the heat transfer behavior is similar to that of single-phase flow. The approach is conceptually similar to Lockhart and Martinelli (1949) who used a two-phase multiplier approach to predict the frictional pressure drop in two-phase flow. Palen and Yang (1993) advocate the following general form for the

condensation heat transfer coefficient:

$$Nu = Nu_l F_{tp} \tag{2.31}$$

where F_{tp} is the two-pase multiplier and the base single-phase heat transfer correlation Nu_l is given by

$$Nu_l = C_l Re_l{}^r Pr_l{}^s \tag{2.32}$$

The two-phase multiplier can be expressed as a function of quality, viscosity ratio, density ratio etc. One possible grouping for the relevant parameters is the Lockhart-Martinelli parameter X defined in Equation 2.28.

Akers and Rosson (1960) give a correlation which can be expressed in terms of Equation 2.31 as

$$C_l = 0.026, \tag{2.33}$$

$$r = 0.8, \tag{2.34}$$

$$s = 1/3, \tag{2.35}$$

$$F_{tp} = 1 + \left(\frac{\rho_l}{\rho_v}\right)^{0.4} \left(\frac{x}{1-x}\right)^{0.8}. \tag{2.36}$$

This is suggested for $Re_v(\rho_l/\rho_v)^{1/2} > 20,000$ and $Re_l > 5,000$.

Shah (1979) compiled a data set that includes 473 shear-dominated flow experiments from 21 independent studies in the open literature to come up with a correlation of the form:

$$C_l = 0.023, \tag{2.37}$$

$$r = 0.8, \tag{2.38}$$

$$s = 0.4, \tag{2.39}$$

$$F_{tp} = 1 + \frac{3.8}{P_{red}{}^{0.38}} \left(\frac{x}{1-x}\right)^{0.76}. \tag{2.40}$$

Palen and Yang (1993) recommends representing the two-phase multiplier as a power of ${\phi_l}^2$, the pressure dop multiplier postulated by Lockhart and Martinelli:

$$F_{tp} = \left({\phi_l}^2\right)^m, \tag{2.41}$$

where

$${\phi_l}^2 = 1 + \frac{C}{X_{tt}} + \frac{1}{{X_{tt}}^2} \tag{2.42}$$

and

$$X_{tt} = \left(\frac{1-x}{x}\right)^{0.9} \left(\frac{\rho_v}{\rho_l}\right)^{0.5} \left(\frac{\mu_l}{\mu_v}\right)^{0.1} \tag{2.43}$$

Carey (1992) recommends the constants:

$$C_l = 0.28, \tag{2.44}$$

$$C = 20, \tag{2.45}$$

$$r = 0.9, \tag{2.46}$$

$$s = 0.5, \tag{2.47}$$

$$m = 0.5. \tag{2.48}$$

Dobson (1994) studied condensing refrigerants, namely R12, R22, R134a, and mixtures of R32 and R125, in 3.14-mm to 7.04-mm tubes. Dobson recommends the following

relation which provided ±15% correlation for 96 % of his data points:

$$F_{tp} = 1 + \frac{a}{{X_{tt}}^n}, \tag{2.49}$$

$$a = 2.22, \tag{2.50}$$

$$n = 0.889, \tag{2.51}$$

$$C_l = 0.023, \tag{2.52}$$

$$r = 0.8, \tag{2.53}$$

$$s = 0.4. \tag{2.54}$$

Heun (1995) speculates that an alternative Lockhart-Martinelli parameter might be more suitable for heat transfer data. This is derived in a manner similar to Lockhart and Martinelli to be:

$$X_{tt,q} = \left(\frac{1-x}{x}\right)^{0.4} \left(\frac{C_{p,l}}{C_{p,v}}\right)^{0.2} \left(\frac{\mu_v}{\mu_l}\right)^{0.2} \left(\frac{k_l}{k_v}\right)^{0.3} \tag{2.55}$$

2.6 Microchannel Tubes

The microchannel technology is still relatively new and there are few studies documenting their heat transfer and pressure drop characteristics.

In a series of papers presented at SAE conferences, representatives of the Modine Manufacturing Company document the performance of microchannel condensers Goodremote and Costello (1988); Struss et al. (1989); Struss et al. (1990); Struss and Gabbey (1990); Guntly (1990); Sugihara and Lukas (1990), and Tait et al. (1991). The topics covered in these publications include system charge reduction, condenser miniaturization, heat exchanger corrosion resistance, and performance comparisons for R12, R22, and R134a.

Zietlow (1995) studied the effect of headers on microchannel heat exchanger behavior. Webb and Yang (1995) examined the performance of plain and microfinned extruded aluminium tubes. In the author's research group, Heun (1995) has done an extensive study on performance and optimization of microchannel condensers; Vij (1996) has worked on

the modeling of the two-phase flow of the refrigerant inside the microchannel tube; and Graham (1995) has documented the heat transfer and pressure drop characteristics for single-phase flow in microchannel tubes.

Chapter 3

Experimental Facility

This chapter describes the experimental facility used for heat transfer and pressure drop studies in microchannel tubes. The schematic diagram of the test facility is shown in Figure 3.1. The heart of the experimental facility is the test section which is essentially a counterflow heat exchanger with refrigerant flowing through the microchannel tube and water flowing in an annular region around the tube. The facility can also be used for testing the microchannel tube with water flowing both inside the tube and on the outside. We shall begin by describing the refrigerant loop component by component, then describe the associated water loop and finally comment on the procedure to be used for running experiments with water on both sides of the tube.

3.1 Refrigerant Loop

The refrigerant loop is closed and uses a lubricant-free, positive-displacement pump to circulate the fluid. The various components of the loop are joined by 1/4 in. copper tubing with joints brazed together or connected by means of compression fittings.

We shall now begin describing the various components of the loop.

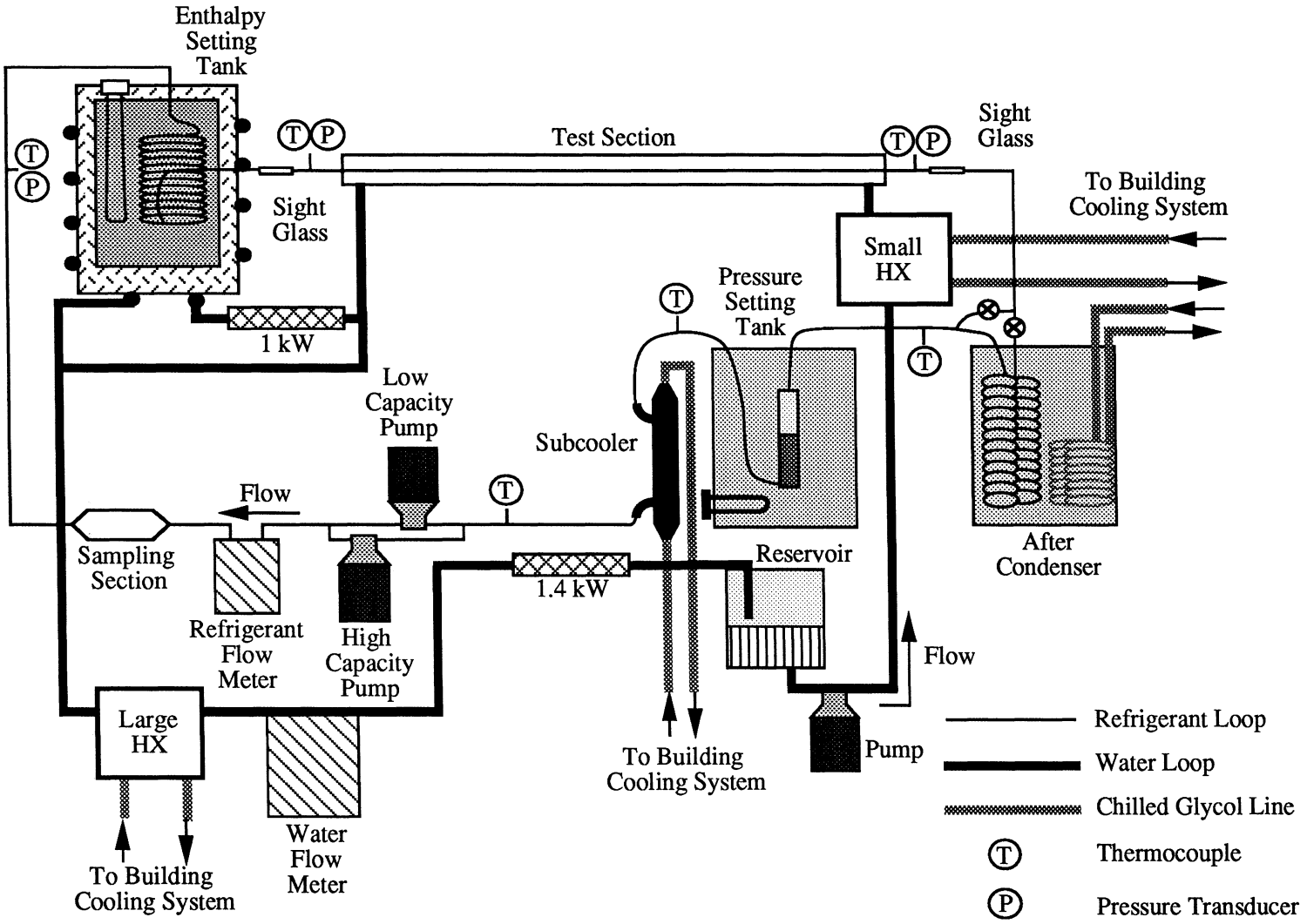

Figure 3.1: Schematic diagram of the experimental facility.

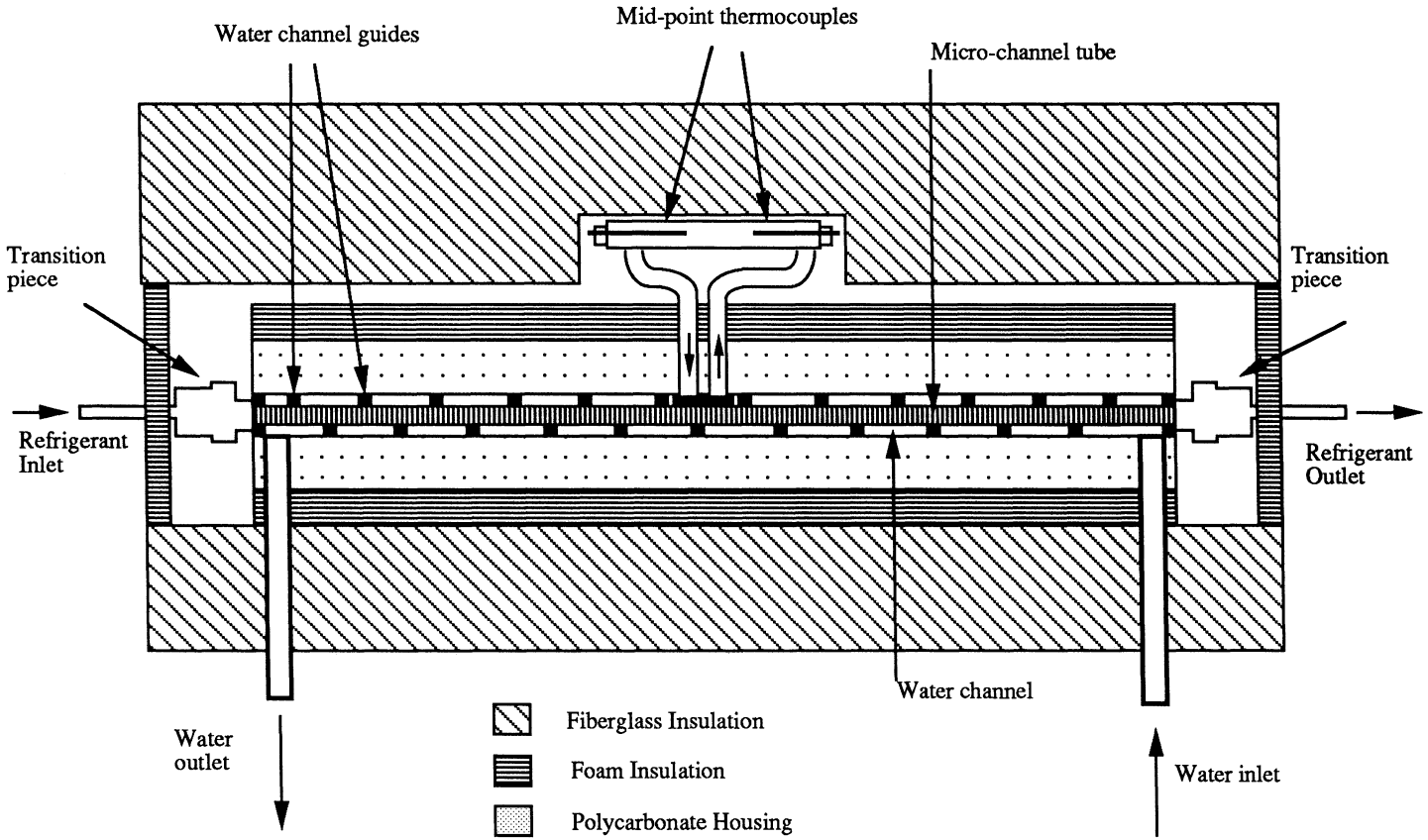

Figure 3.2: Schematic diagram of the test section.

3.1.1 Test Section

The schematic diagram of the test section is shown in Figure 3.2. The test section is a counterflow heat exchanger with refrigerant flowing inside the microchannel tube and water flowing on the outside. The microchannel tube is sandwiched between two polycarbonate sections with grooves cut so that an annular region is formed around the tube through which water can flow. Thin rubber pads are fixed to the grooves with a separation of 1 in. and angle of 45°, so that when the test section is assembled, water has to flow in a spiral path. This is to prevent temperature stratification and to decrease the water-side heat transfer resistance. The arrangement is shown in Figure 3.3. Thermocouples measure the temperature at inlet, outlet and midpoint and also the temperature drop from inlet to midpoint, from midpoint to outlet and from inlet to outlet. The temperature at the mid-point of the test section is measured after diverting the water through a U-tube to ensure proper mixing. For each temperature, a redundant measurement is taken. The polycarbonate housing is covered by foam insulation followed by fiber glass covering in order to minimize the heat loss from the test section.

The microchannel tube is connected to the rest of the refrigerant loop by means of transition pieces which, as the name suggests, provide a transition from the round copper tubing to the flat microchannel tube. A good seal between the tube and the transition piece is achieved by using an O-ring and refrigerant epoxy.

One of the early problems in the loop was that the microchannel tube, made of aluminium alloy, suffered a high rate of corrosion as it was being constantly exposed to hot water on its outside surface. After numerous trials, it was seen that coating the tube with a stainless steel paint succesfully protected the tube.

As on the water side, thermocouples are used to measure the inlet, outlet refrigerant temperature and the temperature drop across the tube. Pressure taps are also present at the inlet and outlet of the test section in the refrigerant line.

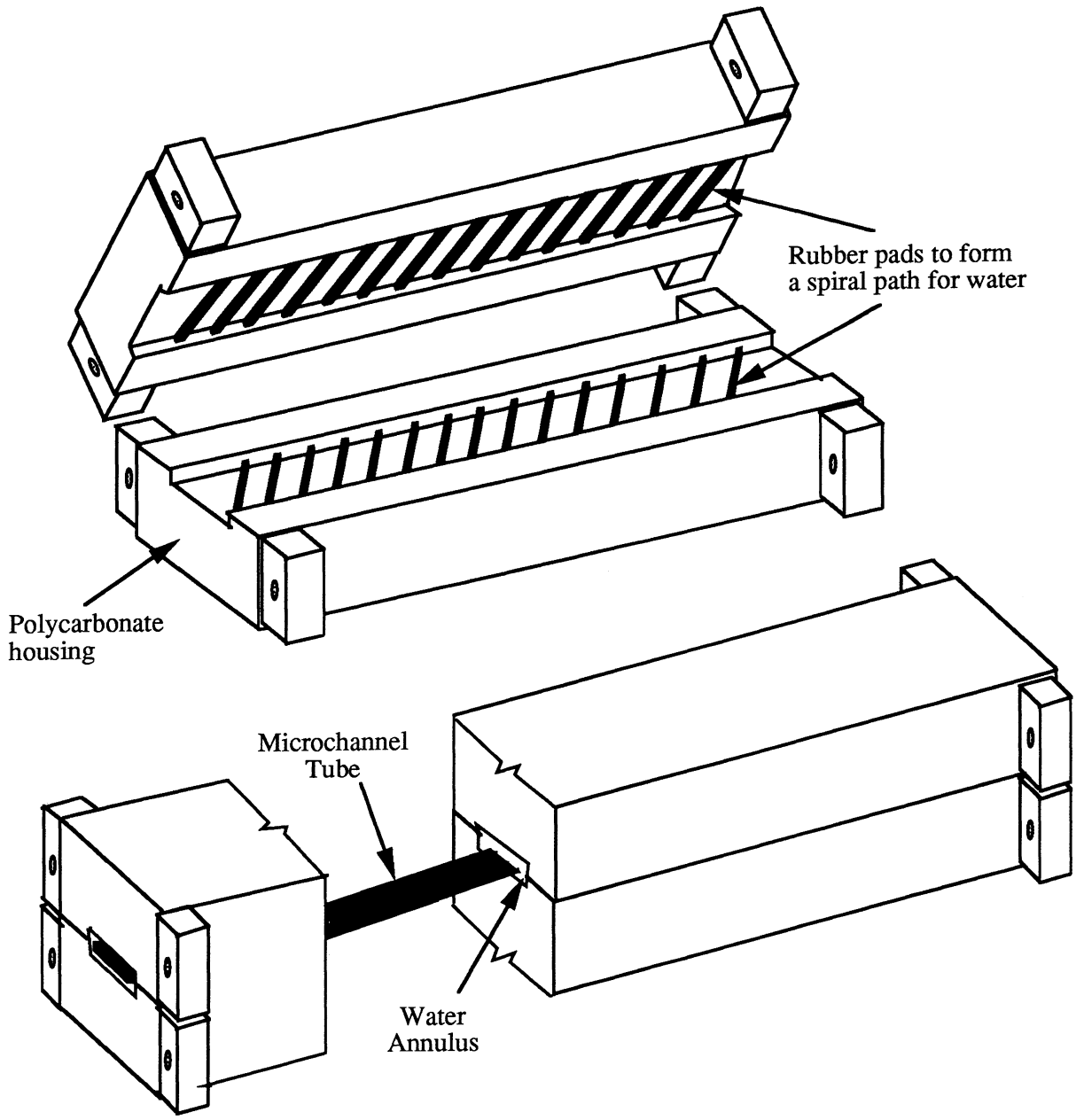

Figure 3.3: Water flow in the test section.

3.1.2 After-condenser

Once the refrigerant passes through the test section, it still might not be fully condensed depending on the test conditions. To ensure full condensation, it is forced to pass through an After-condenser which is a 55-gal stainless-steel drum containing a glycol-water mixture which is kept cold by the system chilled water supply. There is a valve in the refrigerant line that allows one to bypass the After-condenser so that only the required amount of cooling is achieved.

3.1.3 Pressure Regulating Tank

The Pressure Regulating Tank (PRT) is shown in Figure 3.4. Essentially, it has a reservoir in the refrigerant line which is maintained at a constant temperature. The entire reservoir is immersed in a 24-gal tank of glycol-water mixture that has a 2-kW heater controlled by a Capp Model 325 controller. The glycol-water mixture is continously circulated around the tank by means of a submersible pump to improve the mixing and the rate of convection. At steady state, the 2-kW heater is sufficient to maintain the PRT temperature constant; however it takes a long time for the PRT to warm up to that temperature. To accelerate the warming up process, a second heater is provided, which can be switched on manually. There is also a chilled water coil passing through the tank that provides us with a capability to cool the PRT if needed. The tank is insulated by glass wool to reduce heat loss.

Refrigerant enters the PRT from the After-condenser in a slightly sub-cooled state and exits from the bottom of the reservoir so that saturated liquid is delivered. Maintaining two-phase mixture in the PRT allows the loop pressure to be set by controlling the temperature of the PRT. For this purpose, the amount of refrigerant charge in the loop should be such that it is possible to maintain two-phase conditions in the PRT. Too much of charge floods the entire PRT with liquid resulting in higher pressures than that expected by the saturation pressure corresponding to the PRT temperature. By the same

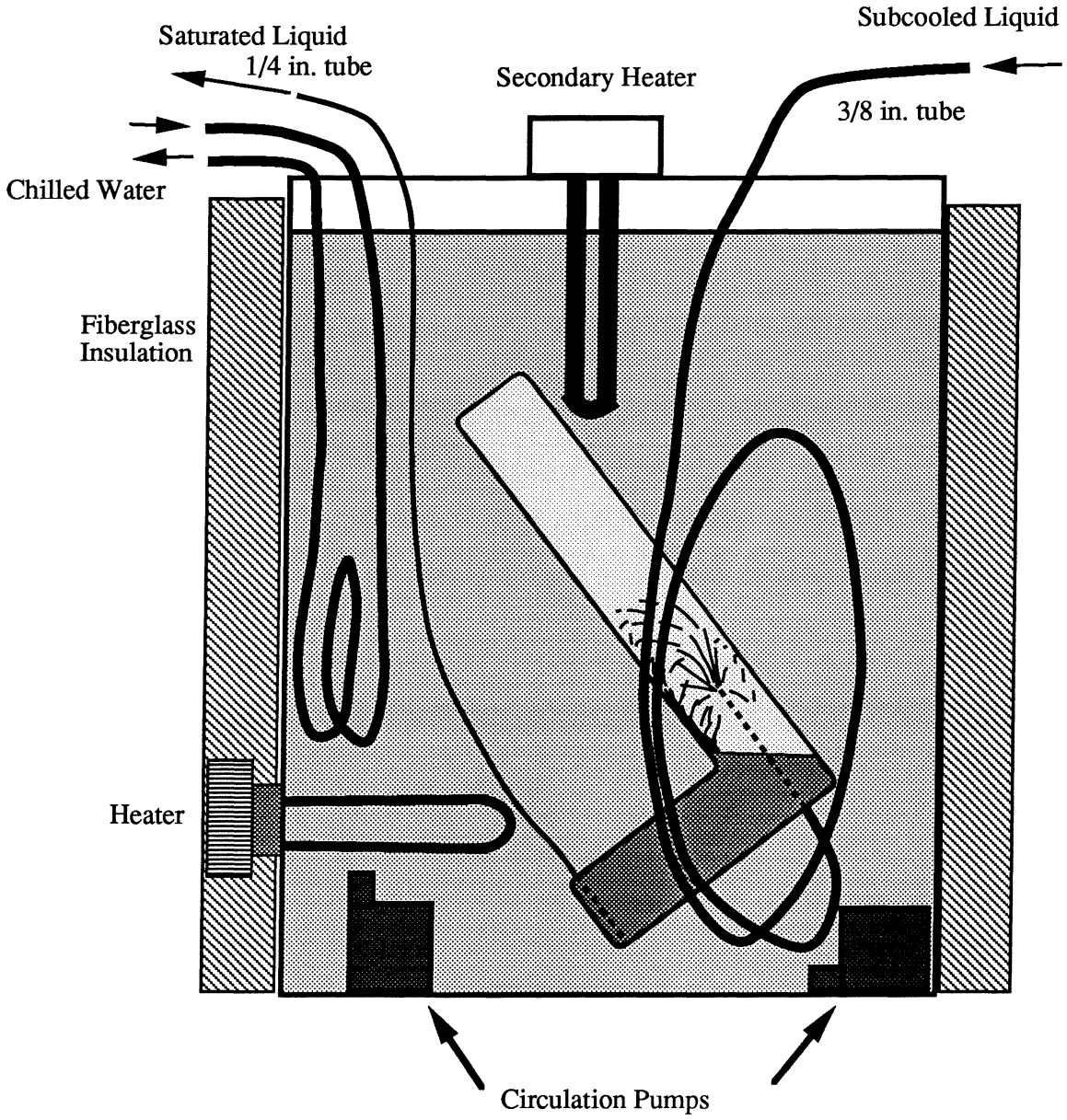

Figure 3.4: Schematic of the Pressure Regulating Tank.

token, too little charge results in lower pressures. Our experience shows that the PRT functions well with around 7 lb of refrigerant in the loop.

The PRT is maintained at a temperature such that the arithmetic mean of the pressures at the inlet and outlet of the test section corresponds to the saturation pressure corresponding to the condensing temperature that has to be tested (125° F in our case).

The PRT also provides the reference temperature for all the thermocouple measurements. An accurate thermistor is used to determine the temperature of the PRT reference temperature.

3.1.4 Subcooler

A subcooler is provided just downstream of the PRT to cool the saturated liquid coming out of the PRT. This is necessary to ensure that there is no vapor present when the refrigerant reaches the pump. The subcooler is a small counterflow heat exchanger that uses the system chilled water supply to sink heat.

3.1.5 Refrigerant Pumps

Lubricant-free, positive-displacement refrigerants pumps were chosen for the refrigerant loop instead of a compressor because a pump allows us to vary and control the oil concentration in the refrigerant. Two pumps have been hooked up in parallel to cover the entire range of flow rate that is desired. Only one pump can be operated at a time. The low-capacity pump is a MICROPUMP® Model 210 driven by a 1/3-hp, variable-speed, DC motor. This pump can handle flow rates up to 2000 lb_m/hr. The high-capacity pump is a MICROPUMP® Model 220 driven by a 1/2-hp, variable-speed, DC motor. A toggle switch connects one of the pumps to the DC voltage controller which in turn is controlled by a Capp Model 535 PID controller. The pump which is not being used is cut off from the rest of the loop by means of ball valves.

Downstream of the pumps, a MICROMOTION Coriolis-effect mass flow meter is used to measure the flow rate of the refrigerant.

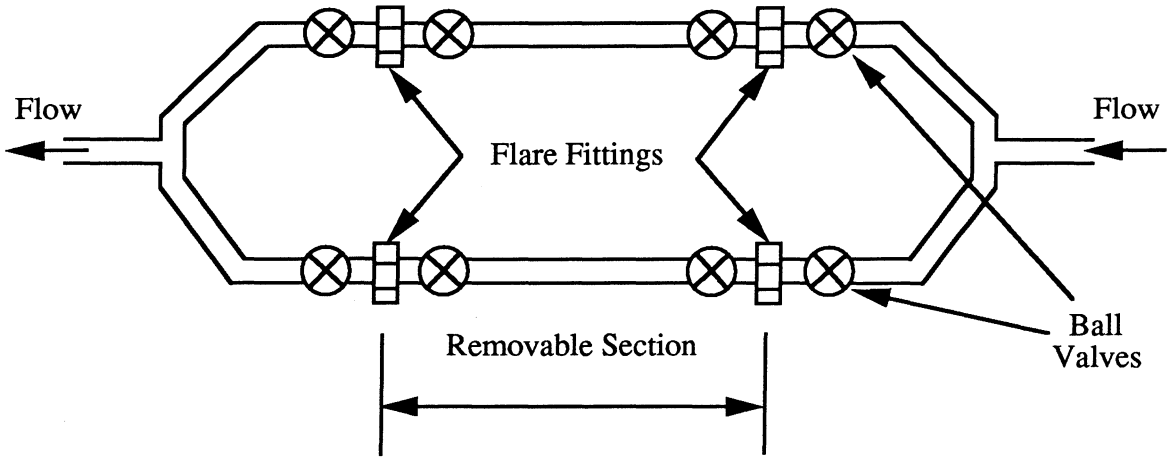

Figure 3.5: Sampling section

3.1.6 Sampling Section

The sampling section provides us with a way of taking a representative sample of refrigerant out of the loop for the purpose of determining its composition and oil measurement. The section is shown in Figure 3.5 and consists of two identical paths of refrigerant. Each path has four ball valves with the inner two valves connected to the outer ones by means of disconnectable flare fittings. One of the paths remains closed during normal operation. When a sample needs to be taken out, the ball valves are turned so that the refrigerant flow is switched to the other path. This causes some refrigerant to be trapped between the valves in the path which has just been cut off. The inner two valves of this path are then disconnected and the sample used for analysis of its composition.

Because the two paths of refrigerant in the sampling section are identical, the flow can be switched from one path to the other without disturbing the conditions in the rest of the loop. This enables us to take samples out without interrupting the experimental run.

3.1.7 Enthalpy Setting Tank

The enthalpy setting tank (EST) shown in Figure 3.6 is used for the purpose of achieving a desired enthalpy of the refrigerant at the inlet of the test section. This is required when two-phase conditions are maintained at the test section inlet, because temperature and pressure are not independent variables in two-phase conditions. To solve this problem, the enthalpy of the fluid is found while it is still in subcooled state (by measuring the temparature and pressure) and then a measured amount of power is added to the refrigerant. Knowing the refrigerant mass flow rate, the enthalpy of the refrigerant at exit can be found by energy balance. This is the purpose served by the EST.

The tank consists of a well-insulated steel drum filled with propylene glycol and water mixture. Refrigerant flows through four parallel coils of copper tubing immersed in the bath. Two submersible pupms circulate the glycol-water mixture in the bath and help to enhance the heat transfer. The power input to the pumps is accounted for in the energy balance. The main heat input is provided by two 6-kW electric heaters.

To minimize the heat loss to the environment, the EST is well insulated. The 24-gal drum is placed inside a larger 55-gal drum and the 4-in. gap between the inner and outer drums is filled with polyurethane insulation. The top of the tank is covered by 1-ft of fibreglass insulation. To furthur reduce heat loss, the outer drum was wrapped with atygon tubing carrying hot water to reduce the temperature gradient. Finally, 4-in. of fibreglass insulation is used to cover the entire drum.

The power added to the heaters is measured using a system developed at the University of Illinois and is described in Meyer (1996). An Ohio Semitronics G-5 watt transducer is used to measure the power dissipated by the submersible pumps. The power measurement is fed as an input to a Capp Model 535 PID controller which continously adjusts the on-time of the heaters to maintain a tight control over the enthalpy of the refrigerant entering the test section.

3.2 Water Loop

Water acts as the heat sink fluid for the test section and is circulated around a closed loop by means of a positive displacement pump. Heat exchangers cooled by the system chilled glycol supply serve to bring back the water to the desired conditions before it re-enters the test section. We shall now describe the various parts of the loop one by one.

3.2.1 Guard-Heater

The water exiting the test section is warmed due to the heat it picked from the refrigerant. A part of this water flow is directed to the Guard-heater which furthur heats up the water before it travels in the tygon tubing wrapped around the Enthalpy Setting Tank. The Guard-heater is a simple electric heater. The purpose of circulating hot water around the EST is to reduce the temperature gradient on the EST walls and hence reduce the heat loss to surroundings. The temperature of the water exiting the guard heater is controlled by varying the flow through the heater which, in turn, is determined by opening or closing a bypass valve.

3.2.2 Large Heat Exchanger and Trim Heater

After exiting the test section and the guard heater, the water is cooled down to the temperature desired at the inlet of the test section. This is achieved by means of a large spiral counterflow heat-exchanger that is cooled by the system chilled glycol supply. The amount of cooling is controlled by varying the flow rate of the chilled glycol through a valve. The water is actually overcooled and allowed to pass through a small 1.4-kW electric heater called the Trim Heater where a precise amount of power is added to get the desired water temperature. The power to the Trim Heater is controlled by a Capp Model 535 PID controller. This arrangement is necessary because the large heat exchanger provides only a rough control over the water temperature.

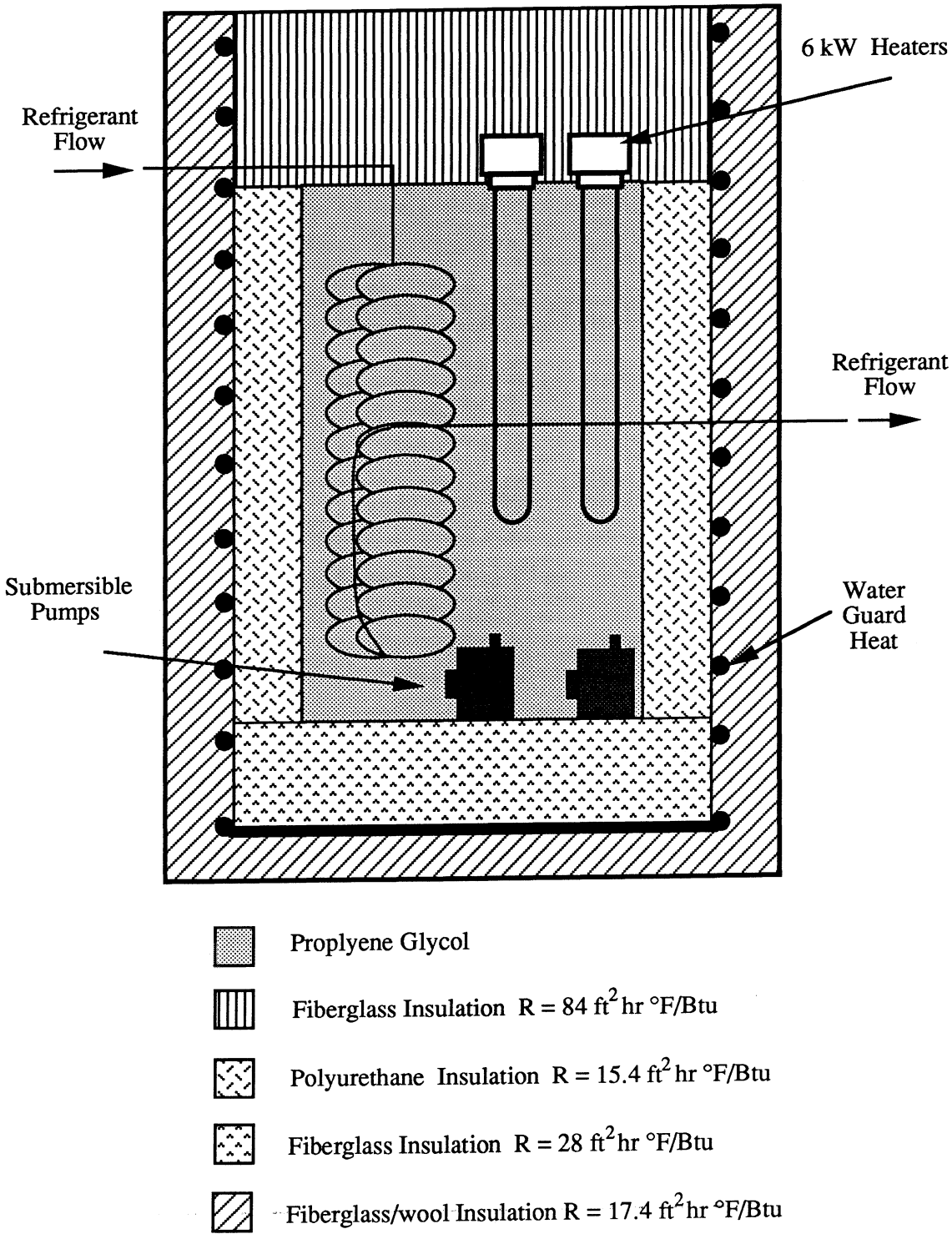

Figure 3.6: Schematic of the Enthalpy Setting Tank.

3.2.3 Reservoir and Water Pump

Water from the Trim Heater empties into a 5-gal reservoir. Immediately below the reservoir is a Teel gear pump which draws the water from the bottom of the tank. A part of the water from the pump outlet is recirculated into the tank so that flow in the main loop can be controlled. Fine control over the water flow is achieved by varying the power to the DC motor which powers the pump. A Capp Model 535 PID controller is used for this purpose.

3.2.4 Small Heat Exchanger

Water exiting the pump unit can be made to pass through a small exchanger cooled by the system chilled glycol supply. This can be used for getting extremely low water temperatures. Water from the exit of this heat-exchanger leads directly to the test section inlet.

3.3 Modifications for Water-Water experiments

The loop has been primarily designed to run with refrigerant flowing inside the microchannel tube and water on the outside. However, some modifications have been made in the loop to allow the microchannel to be tested with water flowing both through the inside and on the outside. This has been used for obtaining additional single phase heat transfer data.

One of the major concerns in making these changes has been to minimize the length of the refrigerant loop which has to be wetted by water while doing the water-water experiments. This is to prevent moisture from being retained in large parts of the loop. As shown in Figure 3.7, three way valves just upstream and downstream of the test section allow the test section to be "switched" from the refrigerant loop to an alternate path. Water from the system supply can then be made to flow through the test section.

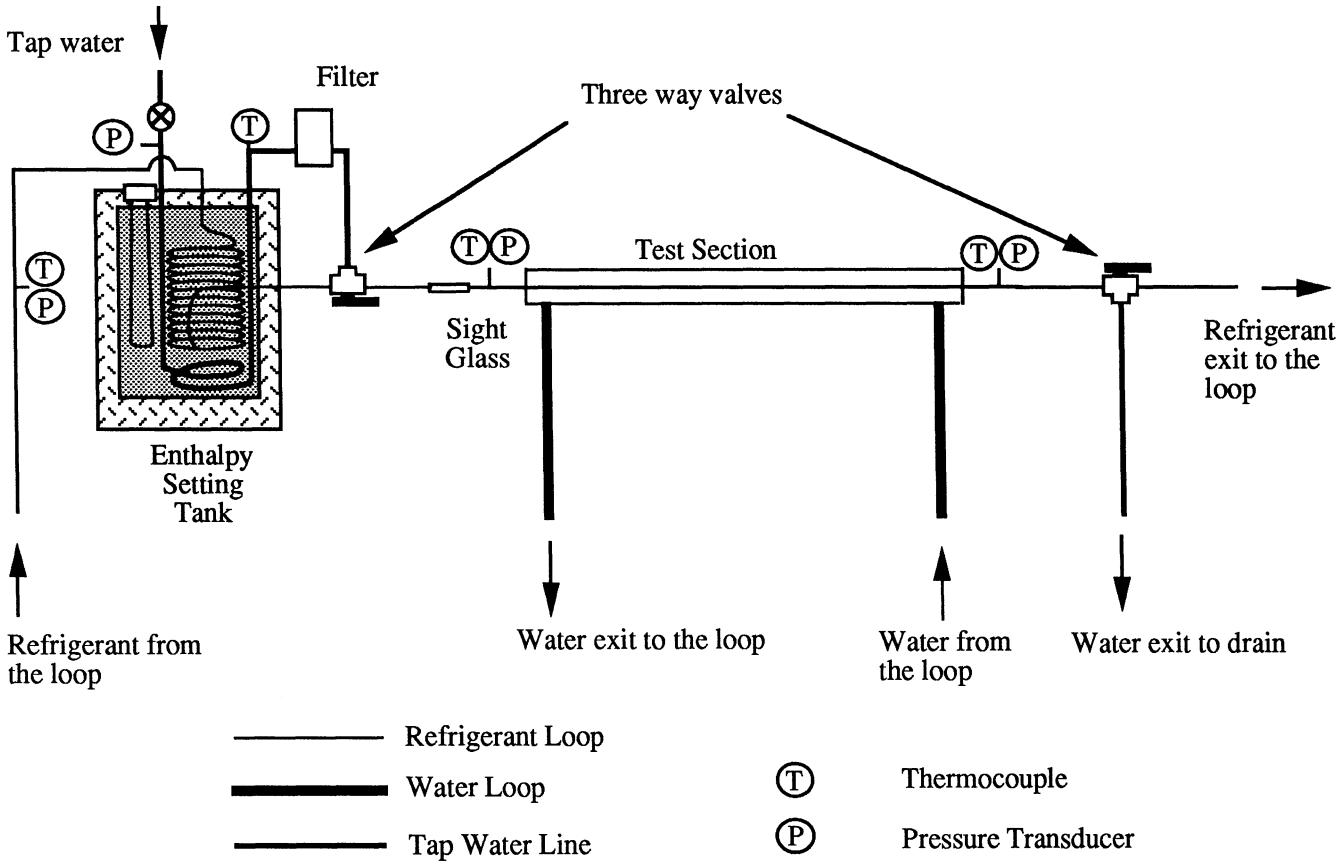

Figure 3.7: Modifications for Water-Water experiments

As in the case of refrigerant, thermocouples measure the temperature of the water at the inlet and the exit of the test section. To get the desired water temperature at the test section inlet, the system water is passed through the Enthalpy Setting Tank through which a regulated amount of heat can be added to it. The flow rate of the water is controlled by means of a pressure regulator. The actual measurement of the flow rate is done by collecting water from the exit in a bucket for a measured period of time and weighing this amount of water. The water from the exit of the test section is discarded into the drain.

3.4 Instrumentation

In this section the instrumentation used in the test facility is described.

3.4.1 Pressure Transducers

Pressure transducers are used to measure the pressure at four points on the refrigerant line as shown in Figure 3.8. Two absolute pressure measurements (one of the measurements is redundant) are taken just upstream of the Enthalpy Setting Tank (EST). This measurement is called the Set Point Pressure and is used to find the enthalpy of the subcooled refrigerant before it enters the EST. Differential pressure transducers measure the pressure drop from the Set Point Pressure to the inlet and the outlet of the test section. The pressure taps are unobtrusive 0.015-in. diameter holes and are connected to the transducers by flexible 1/8-in. copper tubing. To prevent oil from clogging the capillary tubing, the line is kept hot by means of a electric-tape heater. The absolute refrigerant pressure at the test section inlet and outlet is calculated by adding the differential pressures to the Set Point Pressure. The pressure measurements play an important role not only in the calculation of the pressure drop in the microchannel tube but also in determining the refrigerant properties in the test section.

Sensotec Model Number	Location	Range	Accuracy
TJE AP122CD	inlet enthalpy tank	0-500 psia	± 0.5 psi
TJE AP122CD	inlet enthalpy tank	0-500 psia	± 0.5 psi
ZAD122BN	inlet enthalpy tank /outlet test section	0-50 psid	± 0.125 psi
ZAD122BN	inlet enthalpy tank /inlet test section	0-50 psid	± 0.125 psi

Table 3.1: Pressure Transducer Information

All transducers used in the facility are manufactured by Sensotec. Sensor specifications are listed in Table 3.1. The factory calibration of the transducers was verified by using a dead-weight pressure calibration device. As shown in Figure3.9 the slope of the calibration curve agrees very well with the factory calibration. It has been seen that in these pressure transducers the slope of the calibration curve does not change with time but the offset of the curve drifts with age (typically a noticeable change could be observed in two to three weeks). This is attributed to the change in resistance of the strain gauges of the transducer. To correct for the offset, a single-point calibration method was devised which can be conveniently run without taking the transducers out of the refrigerant line. With no refrigerant flow, the pressure in the loop is measured by means of an accurate OMEGA®pressure gauge. The atmospheric pressure is measured by a mercury barometer and added to the pressure gauge reading to get the absolute pressure in the refrigerant loop. Since the pressure in the loop should be the same throughout the loop when the refrigerant is not flowing, this pressure should be equal to the readings shown by the pressure transducers. Any differences in the readings are noted and used to correct the readings of the pressure transducers. The single-point calibration is done once every two to three weeks.

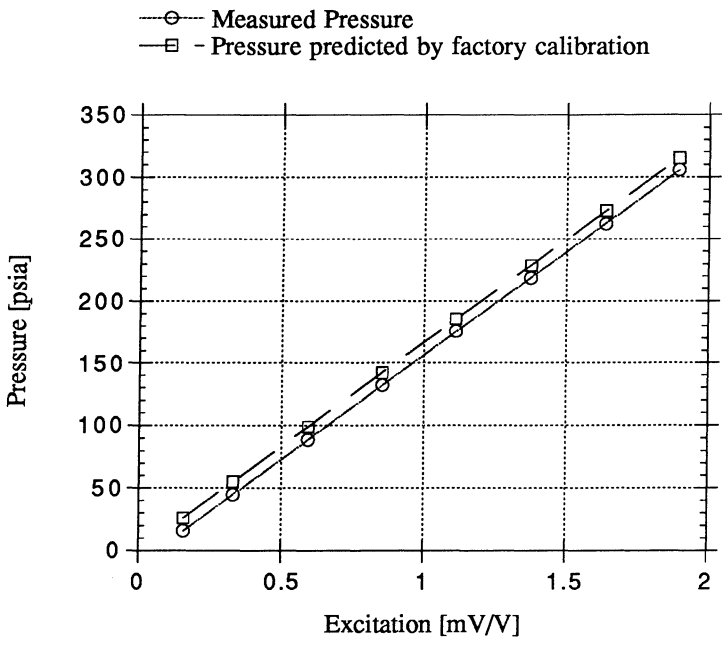

Figure 3.9: Typical calibration curve for a pressure transducer

3.4.2 Temperature Measurement System

The method for making the temperature measurement is shown in Figure 3.10. All the temperatures are measured by Type-T (Copper-Constantan) thermocouples. Three types of measurements are made:

1. Water temperature measurements at the inlet, outlet and midpoint of the test section

2. Refrigerant temperature measurements at the inlet and outlet of the test section, and

3. Other temperatures required for control and monitor information.

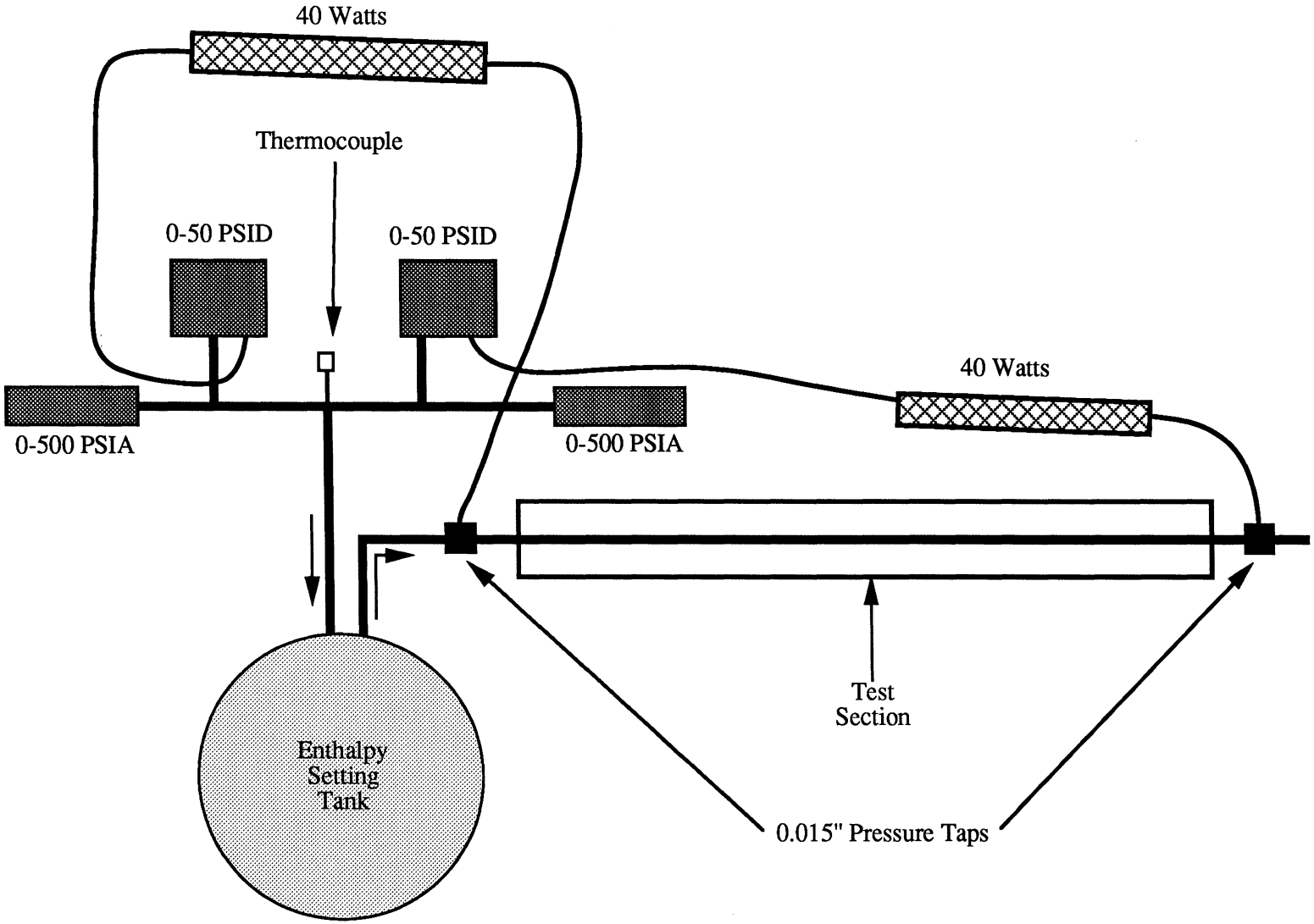

Figure 3.8: Location of the pressure taps in the refrigerant line

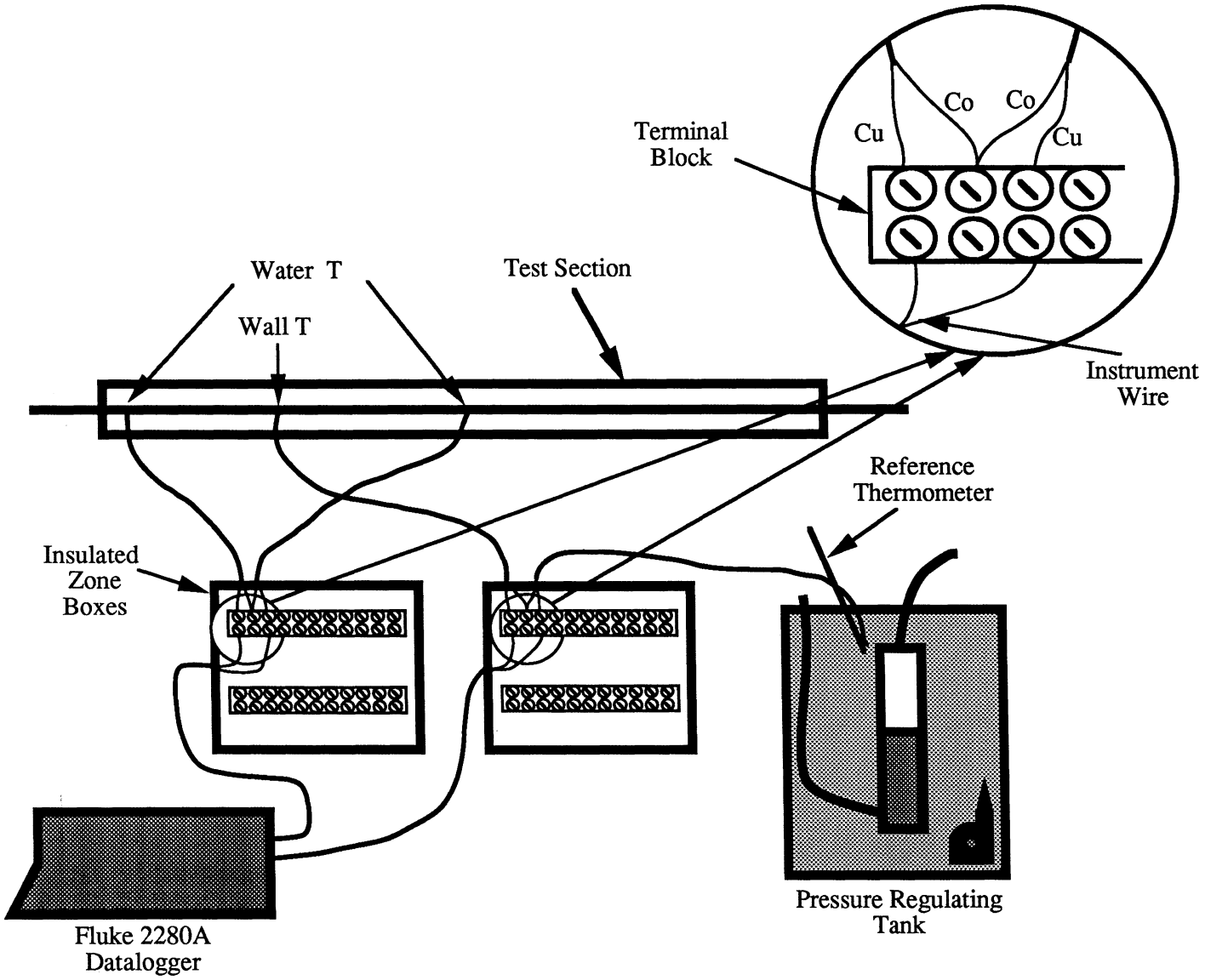

Figure 3.10: Temperature measurement system

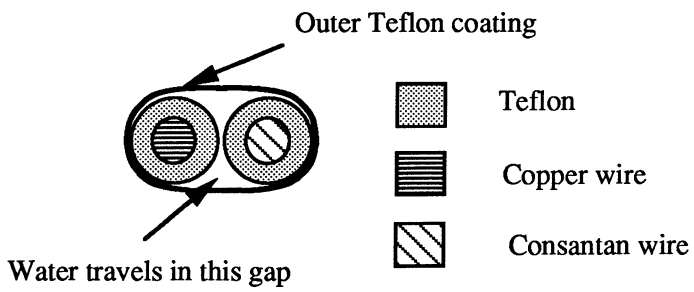

Figure 3.11: Cross-section of the thermocouple wire

Thermocouples require two junctions for each temperature measurement with one junction placed at the the point of interest and the other at a "reference junction" whose temperature is well known. For differential temperature measurements, the two junctions are placed at the points whose differential temperature is to be measured. The reference junction used in our set-up is the Pressure Regulating Tank since it offers a well mixed, nearly isothermal environment. Each thermocouple is then wired to an insulated zone-box where the two leads of the thermocouple are joined as shown in the figure. A shielded copper cable connects the thermocouple leads from the zone-box to the data-logger where the potential difference between the two junctions is measured. The zone-box should be very nearly isothermal to avoid errors in temperature measurement due to the petential differences generated by thermocuple effects inside the zone-box.

An interesting problem arose with the thermocouple leads used to measure the water temperature in the test section. The thermocouple junction used there was originally a simple unshielded bead, with each lead covered by two lawers of Teflon electric insulation as shown in Figure3.11. Water from the test section was able to travel between the outer and the inner Teflon layers by capillary action and drip into the zone-box which was about 10-ft away. This problem was solved by coating the thermocouple junction with a plastic dip and making a tiny break in the teflon layer just few inches after the junction, so that if any water would travel, it would not be carried to the zone-box.

3.4.3 Process Controllers

Various parameters in the test facility must controlled in order to get the desired test conditions. These parameters are: (a) the flow rate of the refrigerant and the water, (b) the temperature of the water at the test section inlet, (c) the power input to the EST and (d) the temperature of the PRT. The parameters are sensed by transducers that provide input to Capp Model 535 PID controllers. Flow rate is controlled by varying the voltage to the armature of the DC motor that powers the pumps. The water temperature at test section inlet is controlled by overcooling the water by a spiral heat exchanger rejecting heat to the system chilled glycol line followed by a small heater whose on-time is controlled by the PID controller.

3.4.4 Mass Flowmeters

The refrigerant mass flow rate is measured by a MicroMotion Model D-12 Coriolis-effect mass-flow-meter with a maximum flow rate of 11 lb/min and a relative accuracy of $\pm 0.2\%$ coupled with an absolute accuracy of ± 0.001 lb/min. The water mass flow rate is measured by a MicroMotion Model D-25 sensor with a maximum flow rate of 45 lb/min and relative accuracy of $\pm 0.2\%$ with absolute accuracy of ± 0.005 lb/min. A MicroMotion Model RFT9712 Remote Flow Transmitter is used to convert the signal from the sensor to milliamps which can then be scanned by the data-logger.

3.5 Data Acquisition System

The various test parameters in the facility are converted into electrical signals and logged by a Fluke 2280A Datalogger. The voltages generated by the thermocouples are measured by Isothermal input connectors and thermocouple/DC voltage scanners. A current input connector and a thermocouple/DC voltage scanner is used to make DC current measurements. The accuracy of the scanner for various kinds of measurements is shown in Table 3.2.

Measurement	Range	Absolute Accuracy	Relative Accuracy
Voltage	± 64 mV	0.008 mV	0.01 %
Voltage	± 512 mV	0.040 mV	0.01 %
Voltage	± 8V	0.800 mV	0.01 %
Voltage	± 64 V	4.0 mV	0.02 %
Current	± 64 mA	0.004 mA	0.25 %

Table 3.2: Fluke 2280A Datalogger scanning accuracy

The data being logged are simultaneously displayed on a computer through a serial interface to the datalogger. The data can be saved and transferred to a Sun workstation for reduction and analysis.

Auxilliary data like the date, refrigerant composition, type of tube being tested, etc are recorded manually and saved in a file along with the main data file. The details of the data reduction procedure are described in the next chapter.

Chapter 4

Experimental Procedure and Data Reduction

This chapter describes the techniques used to prepare the loop for experimentation and the actual procedure used to arrive at the desired test conditions. The data reduction process and the program used to model the test section is also desccribed.

4.1 System Preparation

4.1.1 Leak detection

Before charging the loop with any refrigerant, it must be checked for leaks. This is done by charging the loop with nitrogen to a pressure of about 300 psi and using a soap solution to watch for bubbles at suspected positions. Most of the larger leaks can be easily detected this way. To detect smaller leaks, it helps to isolate different sections of the loop by means of the installed ball valves and watch for a drop in of pressure in any section. The pressure transducers installed on the loop provide an easy way to detect small changes in pressure. Once the leaking section is identified, detailed attention can be focussed on it. Another method of detecting leaks is by charging the loop with a small amount of refrigerant and using an electronic halogen detector to sniff for leaks. These

detectors are very sensitive but can often give misleading observations if care is not taken for proper ventilation and removal of refrigerant "clouds" around the area being tested.

4.1.2 Charging and Discharging

Before charging the loop, it is evacuated and allowed to sit overnight. This allows any residual nitrogen or refrigerant in the loop to be desorbed and pumped out later. Charging is done by heating the refrigerant tank by means of a heat gun to a temperature above the saturation temperature corresponding to the pressure in the loop. Liquid refrigerant is flows from the tank into the loop due to the pressure difference thus developed. The amount of charge being added is monitored by keeping the source cylinder on a scale. The loop takes about 7 lb of charge.

Discharging is done by connecting the loop to a sink cylinder maintained in an ice bath. This takes out all the liquid refrigerant from the loop. The remaining vapor is taken out by means of a vapor recovery unit (Flouromizer Model 6000).

4.2 Conditions for an experimental run

The parameters to be fixed desired for any particular experimental run are: (i) the refrigerant and the water flow rates and (ii) the refrigerant conditions (pressure and temperature) at the inlet of the test section and (ii) the refrigerant conditions at the outlet of the test section.

The flow rates are easily set by means of the PID controllers that control the positive displacement pumps in the loop. The refrigerant flow rate tends to oscillate if the amount of charge in the loop is not correct.

The refrigerant pressure at the inlet is controlled by the temperature of the Pressure Regulating Tank (PRT). The PRT is kept at a temperature such that the arithmetic mean of the inlet and outlet pressures in the test section corresponds to a saturation temperature at 125° F. This can be accomplished by keeping the PRT a few degrees below 125° F.

The refrigerant inlet temperature is controlled by the amount of heat added in the Enthalpy Setting Tank (EST). The EST is a well-insulated bath of glycol-water mixture in which a measured amount of power can be added.

The refrigerant exit temperature or quality is controlled by the amount of heat that is transferred from the refrigerant to the water in the test section. This, in turn, depends on the temperature of the water at the inlet of the test section. The water temperature that gives the right exit conditions for the refrigerant is found by trial and error for each experimental run.

Since both the water loop and the refrigerant loop are closed, a precise amount of heat must be added or removed from the refrigerant and the water so that the required conditions at the test section inlet are maintained. For water, this means that the large heat exchanger that cools the hot water coming from the test section combined with the trim heater should be able to bring the water temperature back to the desired value at the test section inlet. On the other hand, for the refrigerant, the combination of the After Condenser, the PRT and the EST must be able to compensate for the heat lost to the water.

4.3 Issues in achieving steady state

At startup, the PRT is warmed to a temperature of approximately 125° F. A second heater can be switched on manually to accelerate this process. The desired refrigerant flow rate is then set, and the PRT temperature fine tuned to get the required pressures.

4.3.1 Enthalpy setting tank

The EST has a large thermal inertia which makes it difficult to bring it to steady state quickly. Theoritically, we can supply the power required at steady state. The tank will heat gradually eventually raching the proper steady state condition. In practice, this takes an exceedingly long time. Therefore, an alternative approach is used. The correct EST temperature is "guessed" and the EST heated or cooled at the maximum rate to get

that temperature. Once that temperature is achieved, it is checked whether the desired refrigerant inlet temperature is achieved. If not, the EST temperature is decreased or increased accordingly. Once the proper EST temperature is found, the power input to the EST is set so that this temperature can be held constant.

4.3.2 After Condenser

The bypass valve to the After Condenser is set do that slightly subcooled refrigerant enters the PRT. The PRT is then able to deliver saturated liquid at its outlet.

4.3.3 Water inlet temperature

As mentioned earlier, the correct water inlet temperature needed to produce the desired refrigerant exit conditions is found by trial and error. A particular value is "guessed", and the large heat exchanger and trim heater set so that this temperature is maintained. The amount of cooling in the large heat exchanger is controlled by regulating the flow of glycol through it. Care must be taken to wait a sufficiently long time after a change in the setting of the large heat exchanger. This is so because it takes some time for a change to manifest itself in the water inlet temperature.

All the different control parameters are intimately coupled to each other. For example, a change in the PRT temperature changes the boiling temperature in the EST and hence the heat transfer there. A change in EST temperature can change the refrigerant quality in the test section resulting in a change in the test section outlet pressure, which might call for an adjustment of the PRT temperature. Even a change in the water inlet temperature has ramifications on the refrigerant loop causing changes in the EST and the PRT.

The coupling of the various parameters requires that changes in the system be made slowly and sufficient time be allowed for system to respond to that change before further corrective action is contemplated. With experience, the operator learns the response of the various components of the loop and is able to get steady state quickly.

4.4 Data reduction procedure

Once steady state is obtained, data are logged for 5 mins. Auxillary data are recorded manually.

4.4.1 Data reduction program

Data reduction is done in several steps. The raw data are first averaged and outliers rejected. Then they are processed by means of a program which calculates various physical parameters like temperature, pressure, flow rate, etc. from the transducer output. At all stages, the estimates of relative and absolute error are propagated in the calculation using Moffat (1988) method.

The physical parameters for each experimental run are stored in a file. A separate modeling program is then used to predict the heat transfer and pressure drop in the microchannel tube and compare these predicted valueswith the experimental values. This program is also used to find the coefficients in correlations for heat transfer and pressure drop that give best agreement with the experimental data. The modeling program is described in the next section.

4.5 Modeling the test section

The test section is essentially a counterflow heat exchanger with refrigerant flowing through the microchannel tube and water flowing on the outside. For modeling, the test section is discretized into numerous small cells as shown in Figure 4.1. Each cell itself is a counterflow heat exchanger with the outlet of one cell forming the inlet of the neighboring cell. We formulate the equations for each cell and then combine all the equations to solve for the variables of interest. The state variables that we use to describe the physical parameters in each cell are: (i) the pressure and enthalpy for the refrigerant side and (ii) the enthalpy for the water side. The choice of enthalpy as opposed to temperature was made because two-phase conditions inside the tube have be modeled.

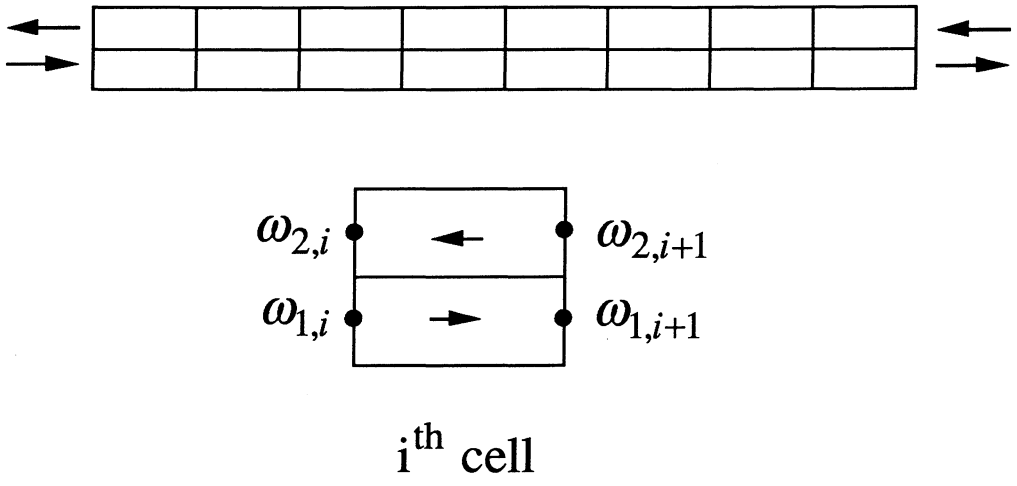

Figure 4.1: Discretization of the test section. ω stands for any property variable

4.5.1 Governing Equations

The governing equations are the familiar mass, momentum and energy balance equations described below:

$$\rho V A = \quad \text{constant} \tag{4.1}$$

$$\frac{d}{dx}\left(\frac{\dot{m}V}{A} + p\right) = -\frac{\rho V^2}{2D_h} f_D \tag{4.2}$$

$$\frac{d}{dx}\left[\dot{m}\left(h + \frac{V^2}{2}\right)\right] = \frac{dq}{dx} \tag{4.3}$$

where $\dot{m}$ is the mass flow rate and A is the free-flow area. The fluid velocity V is the average velocity at a particular cross section. Density variations over the cross-sectional area are assumed to be negligible.

4.5.2 Discretization

The governing equations are discretized for each cell as follows. Consider the cell formed between the i^{th} and the $(i+1)^{th}$ node. Subscript 1 denotes values related to the fluid moving inside the tube and subscript 2 denotes the fluid moving outside the tube. It is assumed that Fluid 2 does not change phase and its properties are not affected by pressure.

The mass balance yields the trivial equations

$$\dot{m}_{1,i} = \dot{m}_{1,i+1} = \dot{m}_1 = \rho_1 V_1 A_1 \tag{4.4}$$

and

$$\dot{m}_{2,i} = \dot{m}_{2,i+1} = \dot{m}_2 = \rho_2 V_2 A_2. \tag{4.5}$$

Replacing V_1 in the momentum equation by $\frac{\dot{m}_1}{\rho_1 A_1}$ gives

$$\frac{d}{dx}\left(\frac{\dot{m}_1^2}{\rho_1 A_1} + p_1\right) = -\frac{\dot{m}_1^2 f_D}{2\rho_1 A_1 D_h}. \tag{4.6}$$

Using a finite volume discretization with the ρ value in the right hand side of the above equation calculated as the mean of the values at the two node we get

$$\left(\frac{\dot{m}_1^2}{\rho_{1,i+1} A_1} - \frac{\dot{m}_1^2}{\rho_{1,i} A_1}\right) + (p_{1,i+1} A_1 - p_{1,i} A_1) = -\frac{\dot{m}_1^2 f_D \Delta x}{2\left(\frac{\rho_{1,i}+\rho_{1,i+1}}{2}\right) A_1 D_h} \tag{4.7}$$

which can be further simplified to

$$p_{1,i+1} = p_{1,i} - \left(\frac{\dot{m}_1^2}{\rho_{1,i+1} {A_1}^2} - \frac{\dot{m}_1^2}{\rho_{1,i} {A_1}^2}\right) - \frac{\dot{m}_1^2 f_D \Delta x}{2\left(\frac{\rho_{1,i}+\rho_{1,i+1}}{2}\right) {A_1}^2 D_h}. \tag{4.8}$$

Neglecting the kinetic energy ($\frac{V^2}{2}$) term in the energy equation, finite volume discretization gives

$$h_{1,i+1} = h_{1,i} + \frac{\Delta q}{\dot{m}_1} \tag{4.9}$$

$$h_{2,i+1} = h_{2,i} + \frac{\Delta q}{\dot{m}_2} \tag{4.10}$$

where the heat transfer Δq for one cell is assumed to be driven by the difference between the arithmetic mean of the hot fluid temperatures and the arithmetic mean of the cold fluid temperatures at the ends of the cell.

$$\Delta q = UA\left(\frac{T_{2,i+1} + T_{2,i}}{2} - \frac{T_{1,i+1} + T_{1,i}}{2}\right) \tag{4.11}$$

Since our state variable is enthalpy rather than the temperature, we wish to express temperature as a function of enthalpy. For single-phase conditions, the temperature can be expressed as a linear function of enthalpy by taking a Taylor series expansion about the old enthalpy value, truncated after the first two terms. This is shown below

$$T(h) = T\left(h^{old}\right) + \left.\frac{dT}{dh}\right|_{h=h^{old}} \left(h - h^{old}\right), \tag{4.12}$$

where h^{old} is the enthalpy at that node in the previous iteration.

This approach reduces the number of iterations required for convergence as the temperature is very nearly a linear function of enthalpy for single-phase. We use the enthalpy as a state variable instead of the temperature even for water because it offers uniformity in setting up the equations in the model and is exactly equivalent to using temperature as the state variable.

Substituting this expression in Equation 4.9, we get

$$\left(1-\frac{UA}{2\dot{m}_1}\left.\frac{dT_1}{dh_1}\right|_{h=h_{1,i}^{old}}\right)h_{1,i}+\left(-1-\frac{UA}{2\dot{m}_1}\left.\frac{dT_1}{dh_1}\right|_{h=h_{1,i+1}^{old}}\right)h_{1,i+1}$$
$$+\left(\frac{UA}{2\dot{m}_1}\left.\frac{dT_2}{dh_2}\right|_{h=h_{2,i}^{old}}\right)h_{2,i}+\left(\frac{UA}{2\dot{m}_1}\left.\frac{dT_2}{dh_2}\right|_{h=h_{2,i+1}^{old}}\right)h_{2,i+1}$$
$$=\frac{UA}{2\dot{m}_1}\Bigg(T_2\left(h_{2,i}^{old}\right)+T_2\left(h_{2,i+1^{old}}\right)-T_1\left(h_{1,i}^{old}\right)-T_1\left(h_{1,i+1}^{old}\right)$$
$$-\left.\frac{dT_1}{dh_1}\right|_{h=h_{1,i}^{old}}h_{1,i}^{old}-\left.\frac{dT_1}{dh_1}\right|_{h=h_{1,i+1}^{old}}h_{1,i+1}^{old}$$
$$+\left.\frac{dT_2}{dh_2}\right|_{h=h_{2,i}^{old}}h_{2,i}^{old}+\left.\frac{dT_2}{dh_2}\right|_{h=h_{2,i+1}^{old}}h_{2,i+1}^{old}\Bigg) \tag{4.13}$$

A similar equation can be obtained by making the substitution in Equation 4.10.

For two-phase conditions, temperature is found from the equation of state

$$T=f(h,p) \tag{4.14}$$

It can be noted that temperature is a function of both enthalpy and pressure for refrigerant mixtures in two-phase conditions.

The quality at the midpoint of the cell is calculated. If the quality lies between 0 and 1, the two-phase relation for temperature is used, otherwise, the single-phase relation is used. The above formulation gives three equations for each cell: one pressure Equation (4.8) and two enthalpy equations (which can be either from the two-phase relations or the single-phase relations). For N cells, we have $3N$ equations and $N+1$ nodes with three variables at each node. Therefore, for solving these equations $3(N+1)-3N=3$ more values are needed. These are: pressure at the inlet of Fluid 1, enthalpy of Fluid 1 at its inlet and enthalpy of Fluid 2 at some point (depending on the strategy used for solving the equations this can be either at the inlet or the exit of Fluid 2).

The strategy for solving for the variables is as follows. First the pressure and enthalpy at all the nodes is estimated by assuming an overall pressure drop and heat transfer rate

and interpolating linearly between the two ends of the test section. For each iteration, the following procedure is adopted:

1. March from the inlet of Fluid 1 and update the pressure at all the nodes using 4.8.
2. Solve for enthalpy values using the new values just obtained for pressure. The method used to update the enthalpy values is described later.
3. Check for convergence in the the pressure and enthalpy values. If convergence is not achieved go to step 1.

4.5.2.1 Updating enthalpy values

Two different strategies were tried for updating the enthalpy values at the nodes.

In the first strategy, the input taken is the enthalpy values of both fluids at the node which forms the inlet of Fluid 1. Then the enthalpy equation is expressed explicitly so that the enthalpy at the node to the right of any node can be calculated. We can thus march along all the nodes updating the enthalpy values at each node.

In the second strategy, the input taken is the enthalpies of the fluids at their respective inlet nodes. The enthalpy equations for each cell are combined to for a set of linear equations that are solved simulataneosly to get the updated values for enthalpy.

The first strategy is simpler and faster to implement but suffers from the fact that it involves integrating the equations for Fluid 2 backward. This was found to result in inaccuracies when the heat exchanger effectiveness of the test section was close to unity. Therefore, the second strategy was adopted.

4.6 Wilson Plot procedure

The modeling program needs the value for UA in each cell. This UA has contributions from both the water-side resistance from outside the tube as well as the refrigerant-side resistance inside the tube. The outside resistance is estimated by a Wilson Plot analysis which is described in this section.

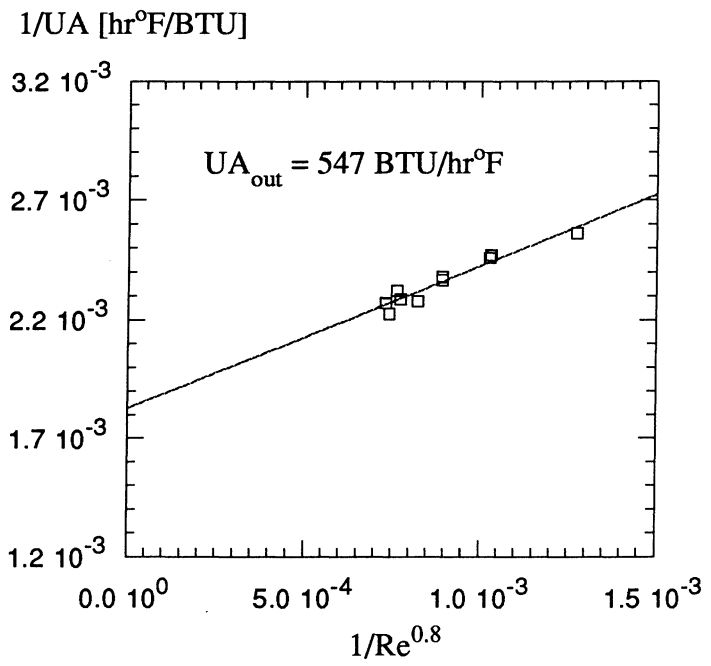

Figure 4.2: A typical Wilson plot.

The overall UA is given by

$$\frac{1}{UA} = \frac{1}{UA_{inside}} + \frac{1}{UA_{outside}} \tag{4.15}$$

UA_{inside} is assumed to be proportional to $Re^{0.8}$. This gives

$$\frac{1}{UA} = \frac{a}{Re^{0.8}} + \frac{1}{UA_{outside}} \tag{4.16}$$

where a is a constant. For Wilson Plot analysis we keep the outside flow rate constant (fixing $UA_{outside}$) and plot $\frac{1}{UA}$ vs. $Re^{-0.8}$ for various inside mass flow rates. A typical Wilson Plot is shown in Figure 4.2. As the Reynolds number increases, the first term in Equation 4.16 approaches zero. Extrapolating the plot to a Reynolds number of ∞ would cause the overall heat transfer resistance to be equal to the outside heat transfer

resistance. Therefore the y intercept of the plot should give us $\frac{1}{UAoutside}$ which is clear from Equation 4.16.

4.7 Heat Loss Tests

Some amount of heat is lost from the water flowing in the annular region of the test section to the surroundings. While this loss is usually well within the acceptable deviation from energy balance, it is still desirable to take it into account. The heat transfer rate UA_{loss} is found by running hot water through the annulus without any flow inside the microchannel tube. At steady state, the drop in the water temperature is indicative of the amount of heat lost to the surroundings. The heat lost divided by the mean temperatue difference between the water and the surroundings gives the UA_{loss} . The value for UA_{loss} was found to be $1.5\frac{kW}{m^2K}$.

Chapter 5

Results

This chapter describes the results of the experiments conducted on microchannel tubes.

5.1 Test conditions

The data has been taken for four different kinds of microchannel tube with the characteristics as shown in Table 5.1.

Three kinds of tests have been conducted for each refrigerant: (a) tests with subcooled liquid throughout the microchannel tube, (b) tests with superheated vapor throughout the tube and (c) tests with full condensation inside the tube. As described earlier, the heat sink fluid used is water which flows in counterflow to the refrigerant. The water flow-rate used in the tests ranges from 1 lb/min to 6.5 lb/min. The water flow-rate has to be low for superheated vapor data and subcooled liquid data because the total amount of heat transferred in the test section for these cases is much less than that for condensing flow. The water-side heat transfer resistance was found experimentally by a Wilson plot technique.

For each of the three types of tests (subcooled liquid, superheated vapor and condensing flow), four different refrigerant flow rates were used. These are 1 lb/min, 1.5 lb/min, 2 lb/min and 2.5 lb/min. For the refrigerant mixture of R-407C the actual composition of the refrigerant inside the loop was checked by gas chromatography analysis and was

Tube type	1	2	3	4
Port shape	Circle	Square	Triangle	Square
# Ports [-]	10	11	13	10
$t_{wall}[mm]$	0.259	0.396	0.309	0.4
$t_{web}[mm]$	0.295	0.251	0.251	0.3
$L_{web}/2[mm]$	0.747	0.607	0.818	0.625
$S_{web}/S_{ref}[-]$	1/2	1/2	2/3	1/2
$D_h[mm]$	1.494	1.214	0.944	1.278
$P[mm]$	46.935	53.38	63.76	50.67
$A_{ref}[mm^2]$	17.53	16.201	15.047	16.19
$L_{HX}[m]$	0.8557	0.8557	0.8557	1.13

Table 5.1: Physical parameters for tubes analyzed in the present study.

found to be 28.6%, 26.7% and 44.6% by weight of R-32, R-125 and R-134a respectively. All tests were done without any oil.

5.2 Heat transfer toefficents for R-22, R-134a and R-407C

Figure 5.1 shows the heat transfer coefficient of liquid refrigerant flowing through the microchannel tube with circular ports plotted vs. the mass flux of the refrigerant. The refrigerants that are compared are R-22, R-134a and R-407C. It is seen that the heat transfer for coefficient for R-22 is slightly higher than that of R-134a whereas that of R-407C is considerably greater.

The comparison for two-phase condensing flow in a circular-port microchannel tube is shown in Figure 5.2. These tests correspond to full condensation inside the microchannel tube. The flow rates tested are the same as mentioned above. The average temperature of the condensing refrigerant was kept around 125°F. The refrigerant enters the microchannel tube as superheated vapor and leaves as subcooled liquid. The onset of condensation is found by assuming the single-phase heat transfer coeffiecient for the vapor region and using the analytical expression for a counterflow heat exchanger to determine

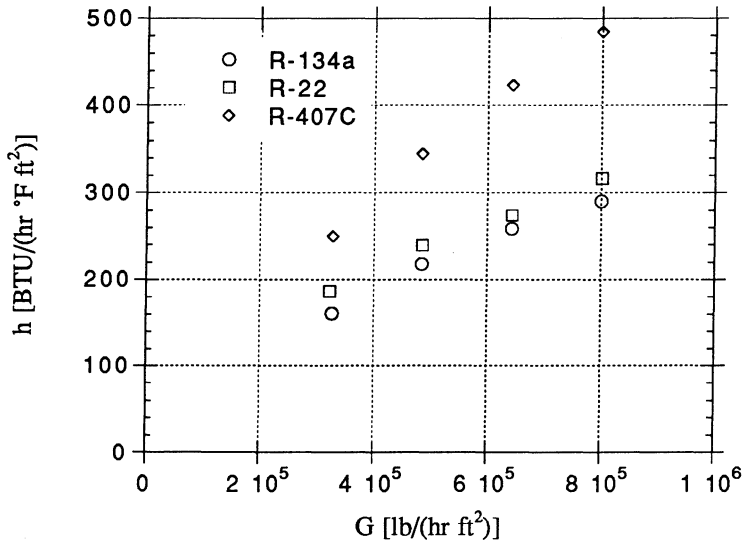

Figure 5.1: Heat transfer coefficient for subcooled liquid flow in a circular-port microchannel tube.

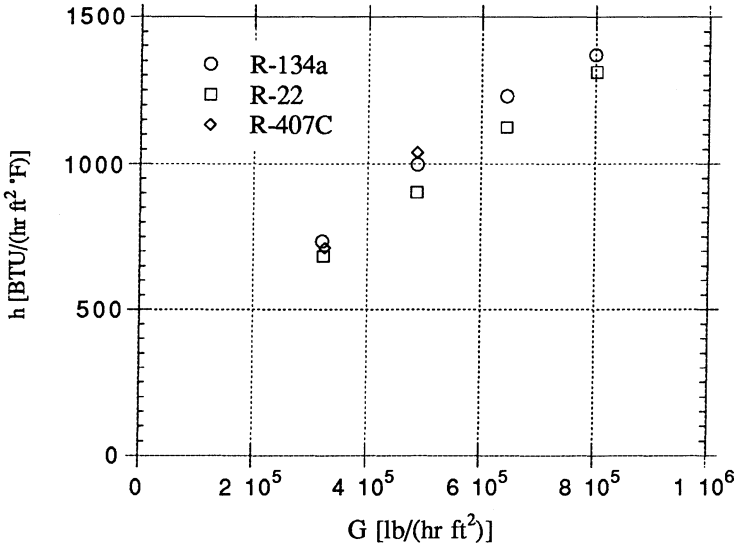

Figure 5.2: Heat transfer coefficient for condensing flow in a circular-port microchannel tube.

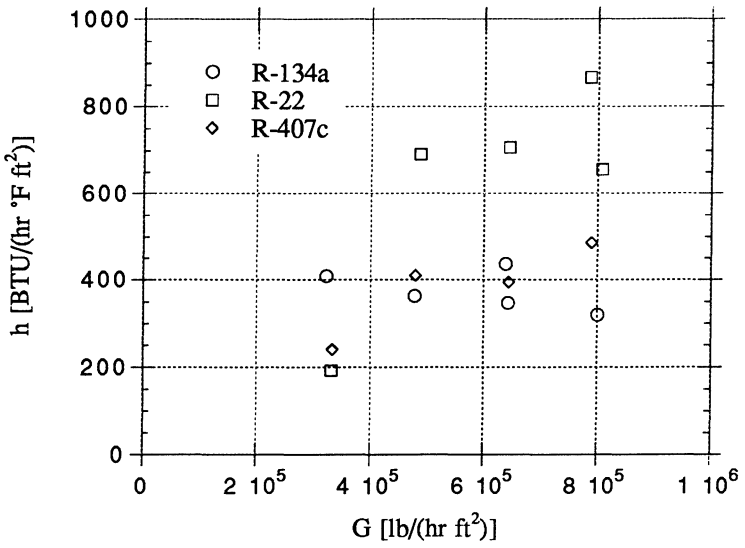

Figure 5.3: Heat transfer coefficient for superheated vapor flow in a circular-port microchannel tube.

the distance along the tube at which the superheated vapor is brought to saturation. In a similar manner, at the other end of the tube, the length of the tube with subcooled liquid flow can be found. The amount of heat transfer and the length of the tube corresponding to the single-phase regions is subtracted from the total heat transfer and the total tube length respectively before extracting the two-phase heat transfer coefficient.

It can be seen from Figure 5.2 that the heat transfer coefficients for the three refrigerants are about the same. The heat transfer coefficient for R-22 appears to be slightly lower than the other two.

Figure 5.3 show the comparision for superheated vapor flowing through the circular-port microchannel tube. The data shows considerable scatter as compared to subcooled liquid and condensing flow data. For superheated vapor the total amount of heat transferred in the test section is not very large due to the lower heat capacity of the vapor which results in low temperature drop along the heat sink fluid resulting in higher uncertainty. Heat loss to the surroundings also forms a considerable fraction of the total heat

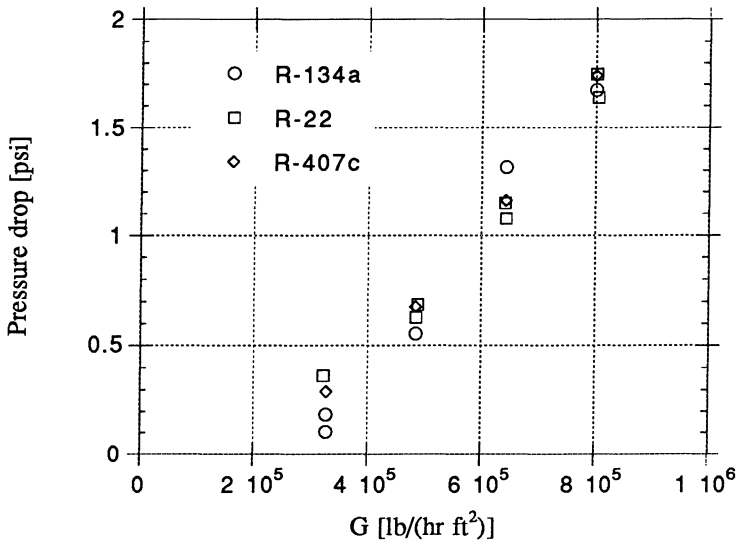

Figure 5.4: Pressure drop for sub-cooled liquid flow in a circular-port microchannel tube.

transfer resulting in a poor energy balance. Finally, with vapor flow the heat exchanger effectiveness of the test section is high which leads to high uncertainties when estimating the heat transfer coefficient from the total heat transfer in the test section.

5.3 Pressure drop data for different refrigerants

Figures 5.4, 5.5 and 5.6 show the pressure drops for subcooled liquid, superheated vapor, and condensing flow, respectively, in a circular-port tube. The subcooled liquid pressure drops are similar for all three refrigerants, but R-134a shows a higher pressure drop in superheated vapor flow and condensing flow.

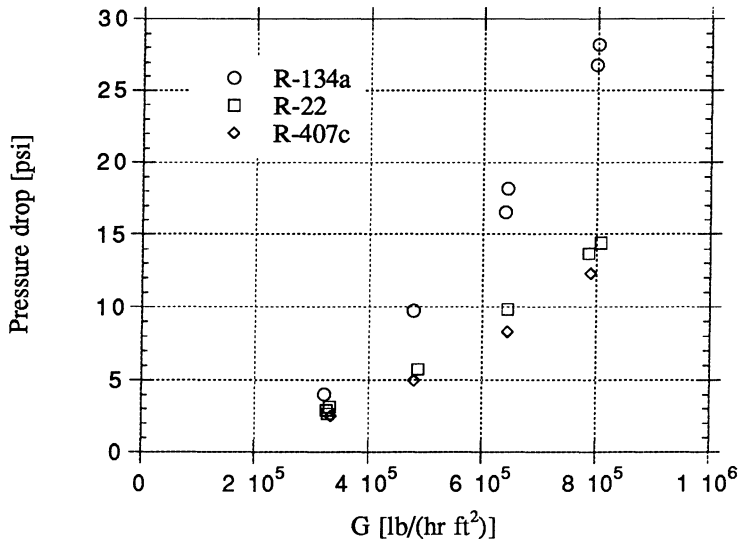

Figure 5.5: Pressure drop for superheated vapor flow in a circular-port microchannel tube.

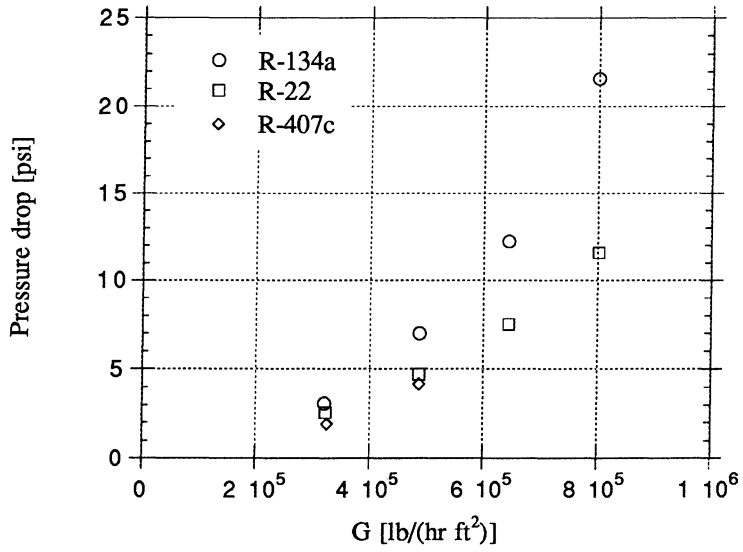

Figure 5.6: Pressure drop for condensing flow in a circular-port microchannel tube.

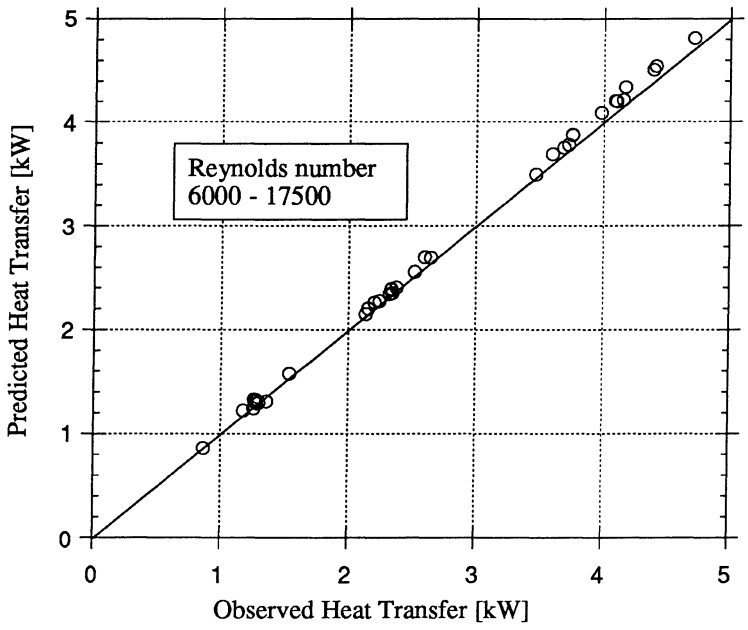

Figure 5.7: Heat Transfer for water flowing through square-port microchannel tube.

5.4 Comparision of data with existing correlations

A test section is modelled as a counterflow heat exchanger as described in Secion 4.5 and the heat transfer and pressure drop are predicted based on existing correlations for single-phase and two-phase flow. This section discusses the comparision of the predicted values with the experimentally measured values.

5.4.1 Single-phase flow

5.4.1.1 Water-water data

For single-phase data, tests were conducted with water flowing both inside as well as outside of the microchannel tube. Figure 5.7 compares the predicted heat transfer with the measured heat transfer for water flowing through a square-port tube (Type 4 in Table 5.1). The Dittus-Boelter (Equation 2.19) correlation is used to estimate the inside heat transfer coefficient. It is seen that the predicted data agrees very well with the observed

Annulus flow rate [lb/min]	% change in Q_{pred} for 5% increase in h	% change in Q_{pred} for 5% decrease in h	HX effectiveness
10	0.363	-0.763	0.5432
5	0.33	-0.707	0.6579
2	0.158	-0.338	0.8868
1	0.028	-0.086	0.9745

Table 5.2: Sensitivity of predicted heat transfer to heat transfer coefficient for water-water data.

data, although the program overpredicts slightly at higher heat transfer rates. However, a sensitivity analysis reveals that the predicted heat transfer is not very sensitive to changes in the inside heat transfer coefficient. The change in the predicted heat transfer for 5% change in the heat transfer coeffecient is shown in Table 5.2. The low sensitivity of the predicted heat transfer is due to two reasons:

1. the overall UA of the heat exchanger, given by

$$UA = \frac{UA_{outside}UA_{inside}}{UA_{outside} + UA_{inside}}, \tag{5.1}$$

   may not be a strong function of UA_{inside} if the ratio $UA_{inside}/UA_{outside}$ is high.

2. Sensitivity of the heat transfer to the overall heat transfer resistance becomes low as the heat exchanger effectiveness gets close to unity.

5.4.1.2 Refrigerant data

As mentioned earlier heat transfer and pressure drop data were taken for circular-port microchannel tube for three different refrigerants. Both superheated vapor data and subcooled liquid data have been taken. Figures 5.8 and 5.9 compares the experimentally determined heat transfer for subcooled liquid data and superheated vapor data, respectively, with heat transfer predicted by our model using the Dittus-Boelter correlation. The agreement between the predicted and the experimental values is good. The same

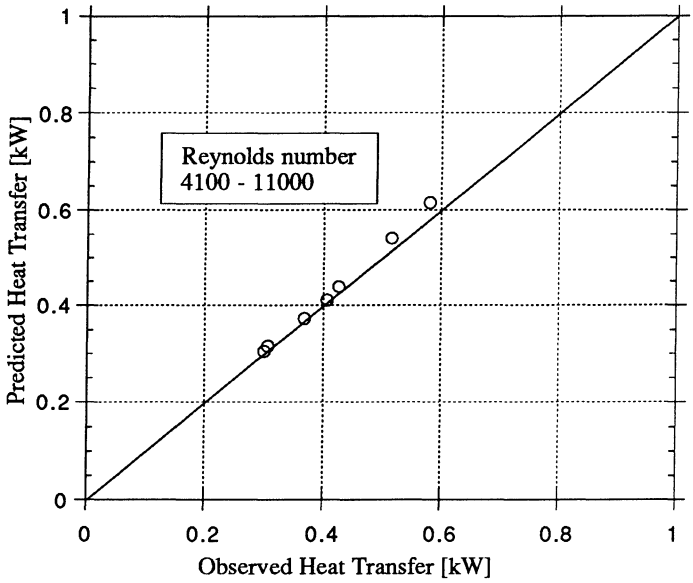

Figure 5.8: Heat Transfer for subcooled R-22 flowing through a circular-port microchannel tube.

comparision is repeated for R-134a in Figures 5.10 and 5.11. Figures 5.12 and 5.13 show the corresponding plots for R-407C.

The comparision of the predicted pressure drop and the experimentally measured pressure drop for the circular microchannel tube is shown in the Figures 5.14, 5.15, 5.16, 5.17, 5.18 and 5.19.

The pressure drop data for subcooled and superheated R-22 show good agreement with the experimental results. Here, a modified form of the Churchill correletion (Equation 2.15) has been used to estimate the friction factor for single-phase flow. The plot for subcooled R-134a also shows good agreement with experiment, but the pressure drop for vapor R-134a flowing through the circular-port microchannel tube are underpredicted. This discrepancy could not be resolved. The predicted pressure drop for R-407C agree with experimental results.

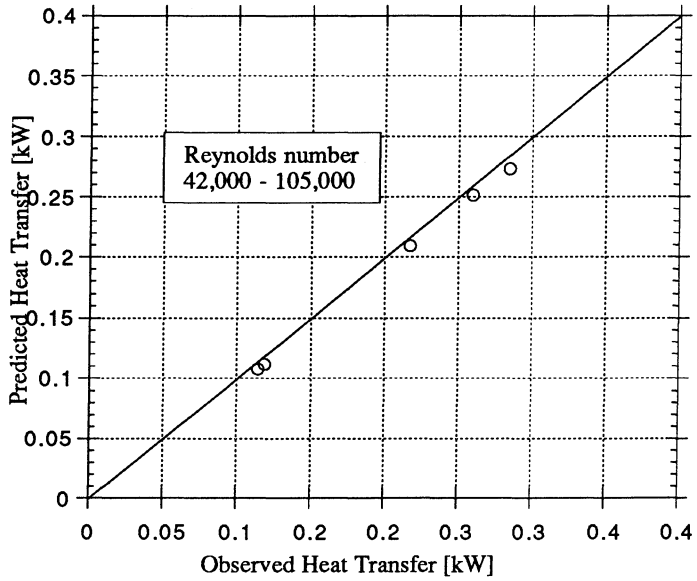

Figure 5.9: Heat Transfer for superheated R-22 flowing through a circular-port microchannel tube.

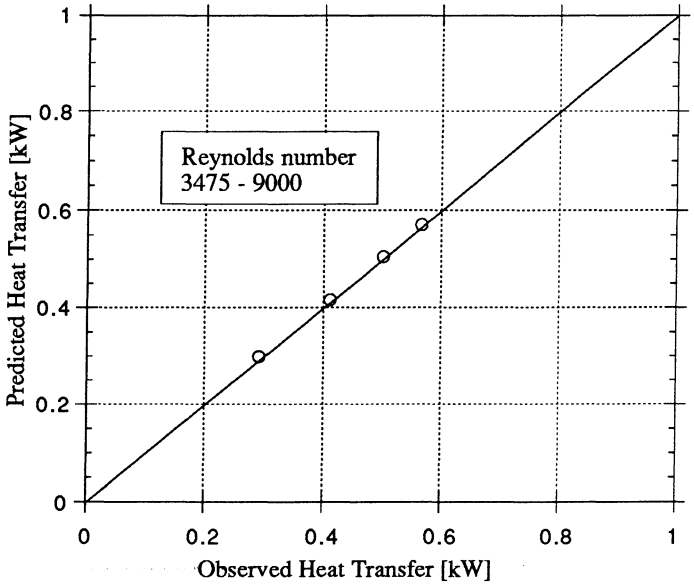

Figure 5.10: Heat Transfer for subcooled R-134a flowing through a circular-port microchannel tube.

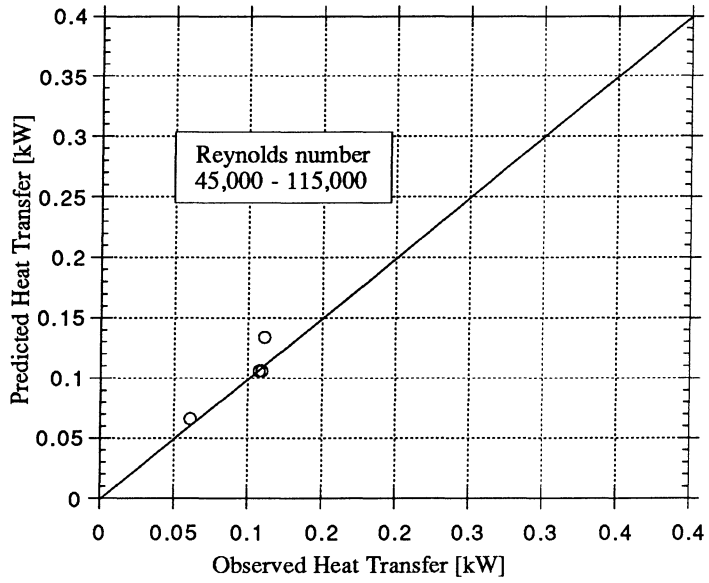

Figure 5.11: Heat Transfer for superheated R-134a flowing through a circular-port microchannel tube.

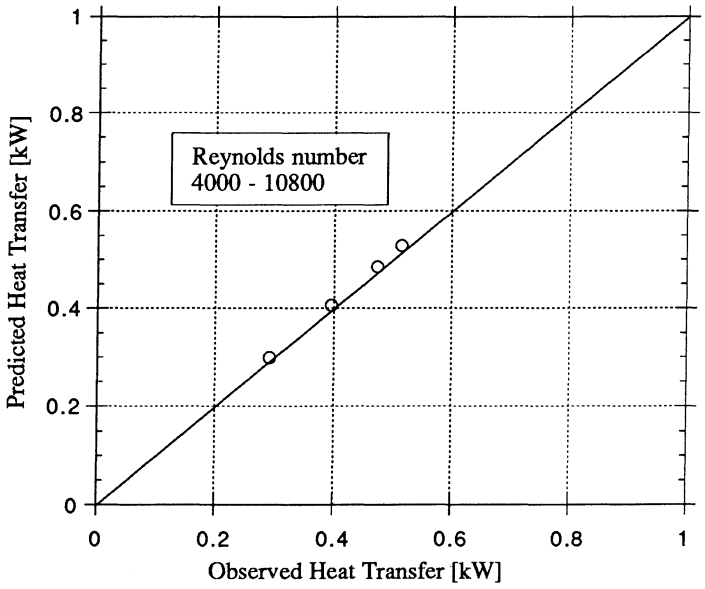

Figure 5.12: Heat Transfer for subcooled R-407C flowing through a circular-port microchannel tube.

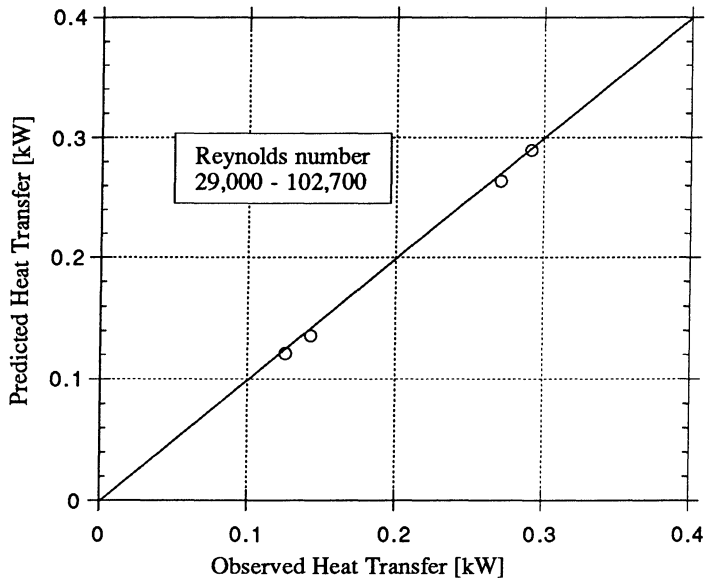

Figure 5.13: Heat Transfer for superheated R-407C flowing through a circular-port microchannel tube.

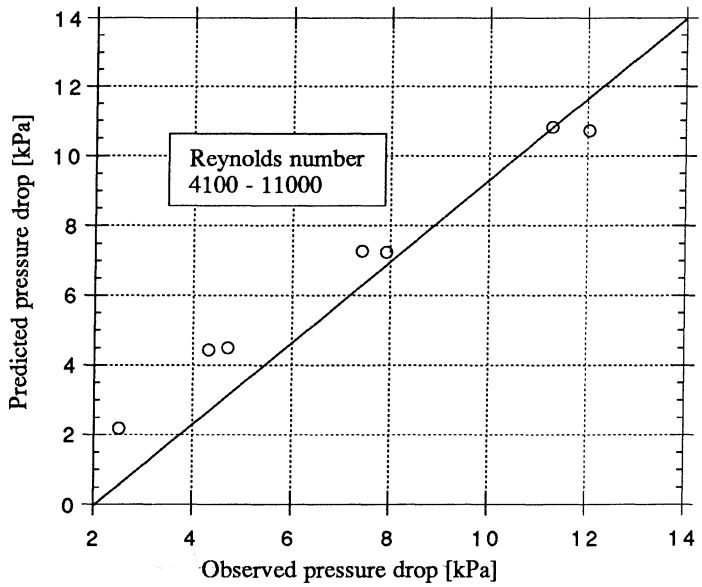

Figure 5.14: Pressure drop for subcooled R-22 flowing through a circular-port microchannel tube.

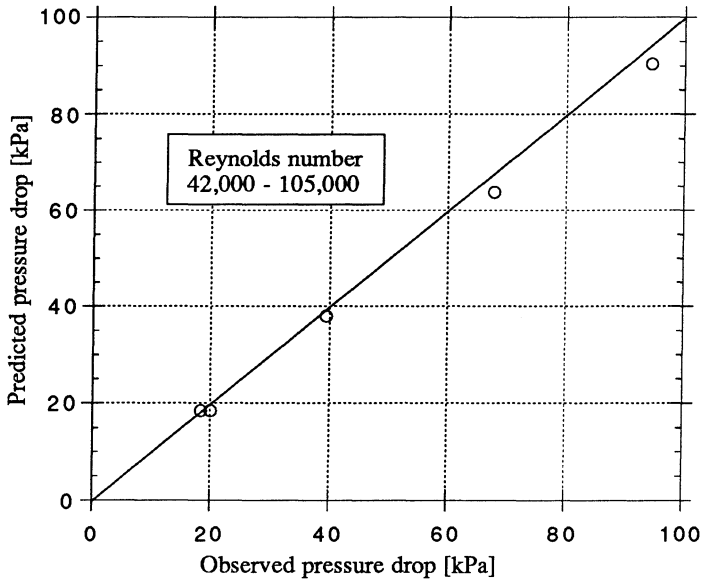

Figure 5.15: Pressure drop for superheated R-22 flowing through a circular-port microchannel tube.

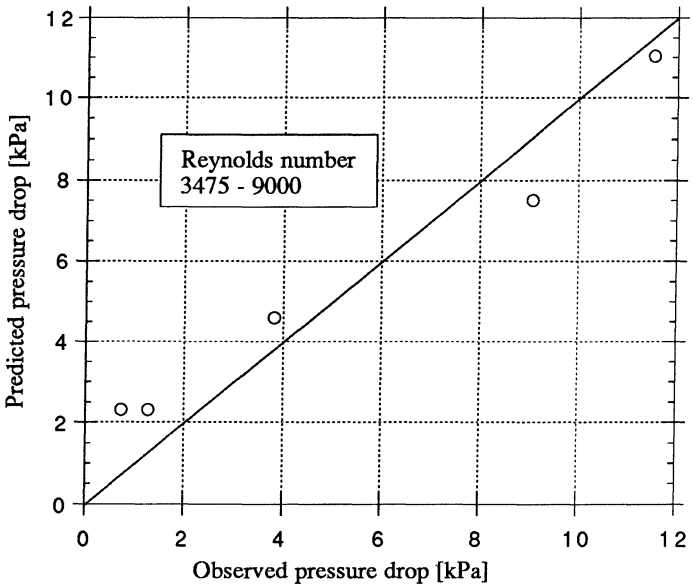

Figure 5.16: Pressure drop for subcooled R-134a flowing through a circular-port microchannel tube.

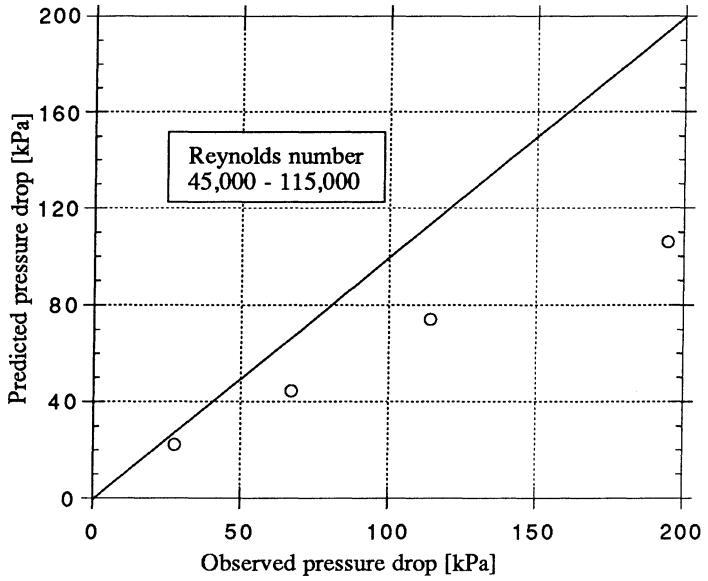

Figure 5.17: Pressure drop for superheated R-134a flowing through a circular-port microchannel tube.

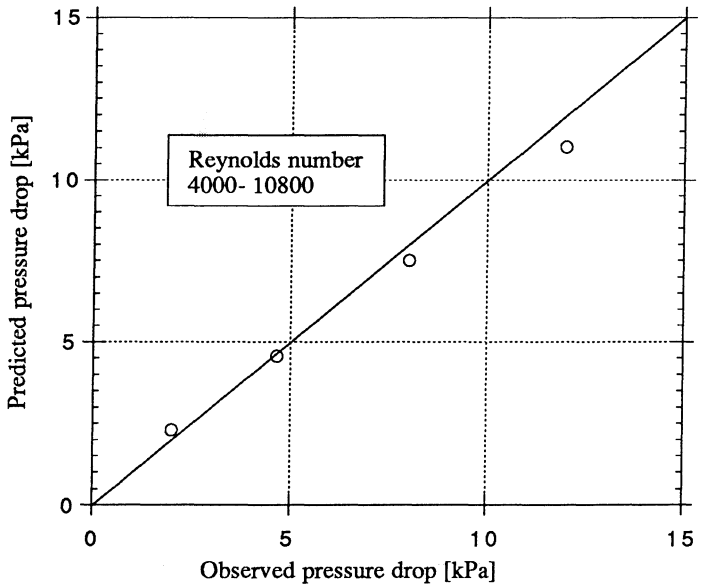

Figure 5.18: Pressure drop for subcooled R-407C flowing through a circular-port microchannel tube.

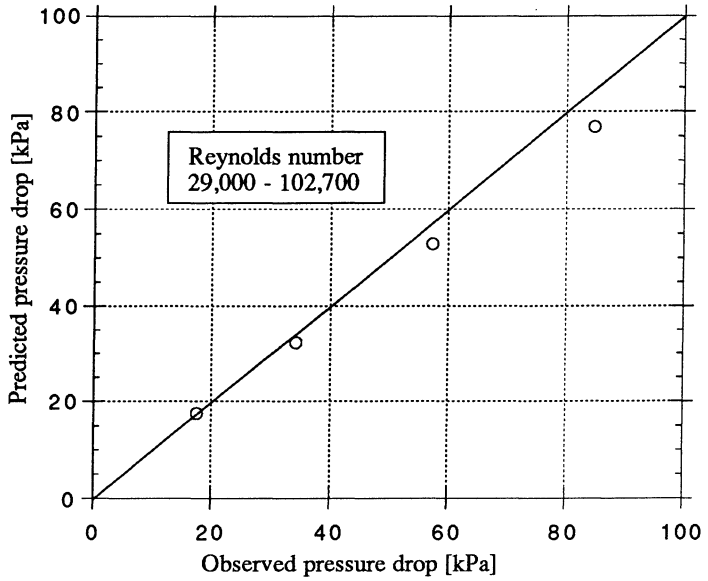

Figure 5.19: Pressure drop for superheated R-407C flowing through a circular-port microchannel tube.

5.4.2 Two-phase data

The heat transfer and pressure drop plots for R-22 and R-134a condensing in a circular-port microchannel tube are shown in Figures 5.20, 5.21, 5.22 and 5.23. The Dittus-Boelter correlation is used for single-phase heat transfer coefficient and the Dobson two-phase multiplier correlation (Equations 2.54) is used for two-phase heat transfer correlation. The two-phase pressure drop is estimated by the Lockhart-Martinelli parameter using Equation 2.29.

The predicted heat transfer data agree well with the experimental results, but the pressure drop data are overpredicted.

5.4.3 Refrigerant data for square-port tubes

It is interesting to study data taken for square-port microchannel tube as opposed to circular-port tubes. Figures 5.24 and 5.25 show the heat transfer and pressure drop for subcooled R-22 flowing through a square-port microchannel tube (Tube 2 in Table 5.1).

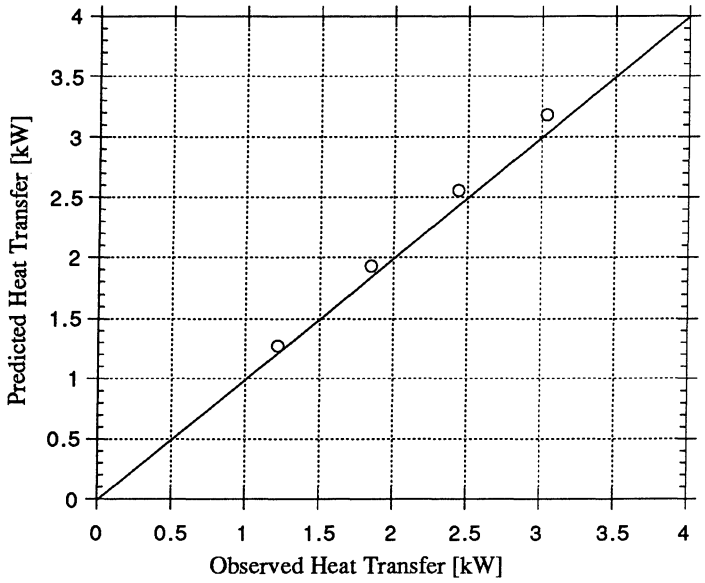

Figure 5.20: Heat Transfer for condensing R-22 flowing through a circular-port microchannel tube.

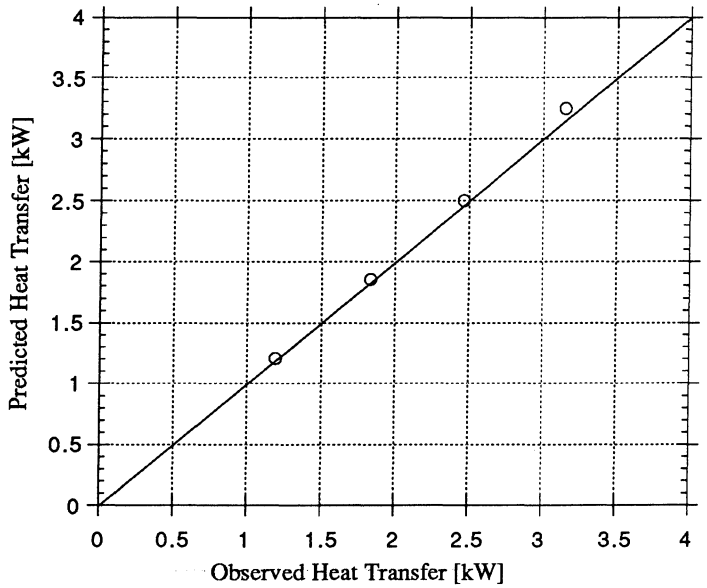

Figure 5.21: Heat Transfer for condensing R-134a flowing through a circular-port microchannel tube.

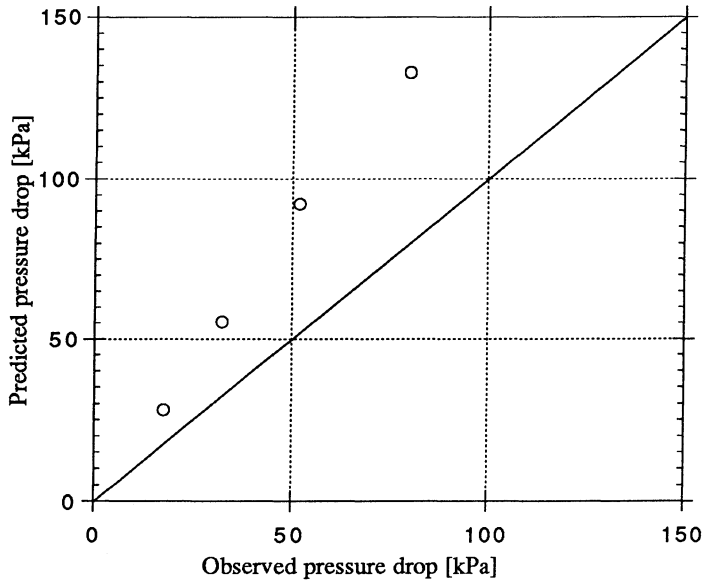

Figure 5.22: Pressure drop for condensing R-22 flowing through a circular-port microchannel tube.

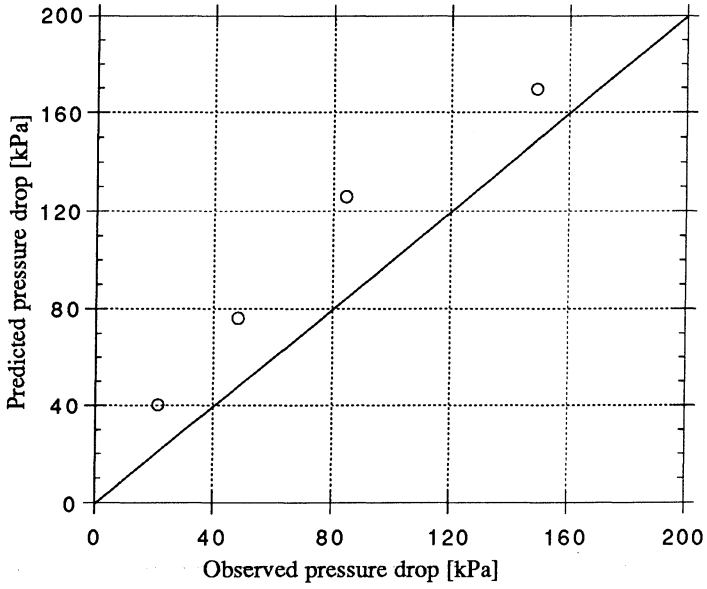

Figure 5.23: Pressure drop for condensing R-134a flowing through a circular-port microchannel tube.

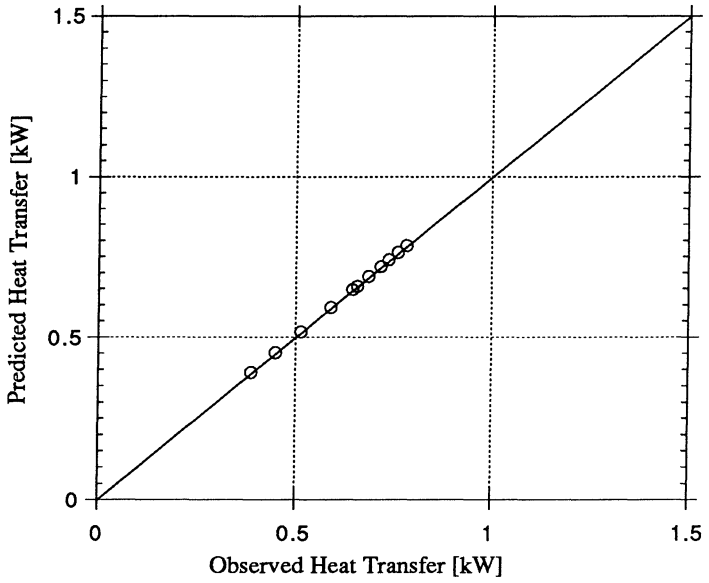

Figure 5.24: Heat Transfer for subcooled R-22 flowing through a sqaure-port microchannel tube.

The predicted data agree well with the experimental data. The correlations used for the square-port tube are the same as that for the circular-port tube with the hydraulic diameter measured by previous nitrogen flow tests. The Nusselt number and the Reynolds number are based on this hydraulic diameter.

Figures 5.26 and 5.27 show the heat transfer and pressure drop for R-22 condensing in a square-port microchannel tube. It is seen that both the heat transfer and pressure drop are overpredicted by our model.

5.4.4 Sensitivity analysis

A sensitivity analysis was carried out to see the effect of changing the refrigerant-side heat transfer coefficient on the total heat transfer. As for the water-water data, it is seen that the total heat transfer is not very sensitive to the heat transfer coefficent. On average, for two-phase heat transfer coefficient, a change of 10 % results in a change of only 2 %. For a similar change in the heat transfer coefficient in single-phase flow, the

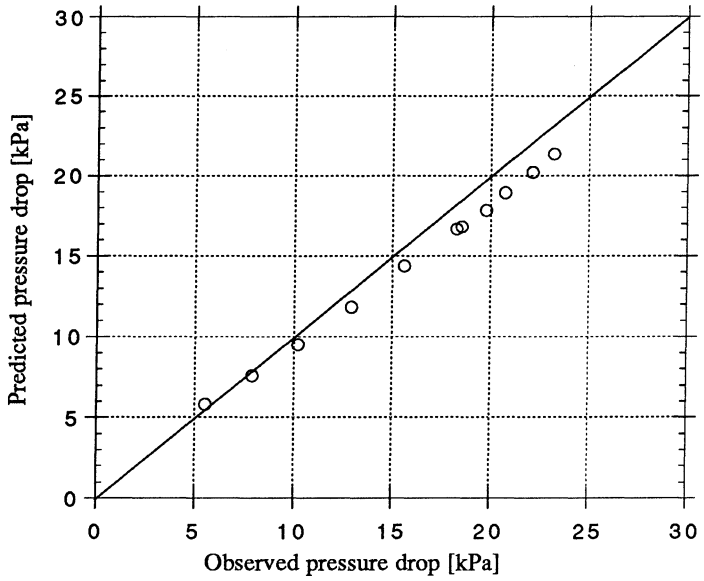

Figure 5.25: Pressure drop for subcooled R-22 flowing through a square-port microchannel tube.

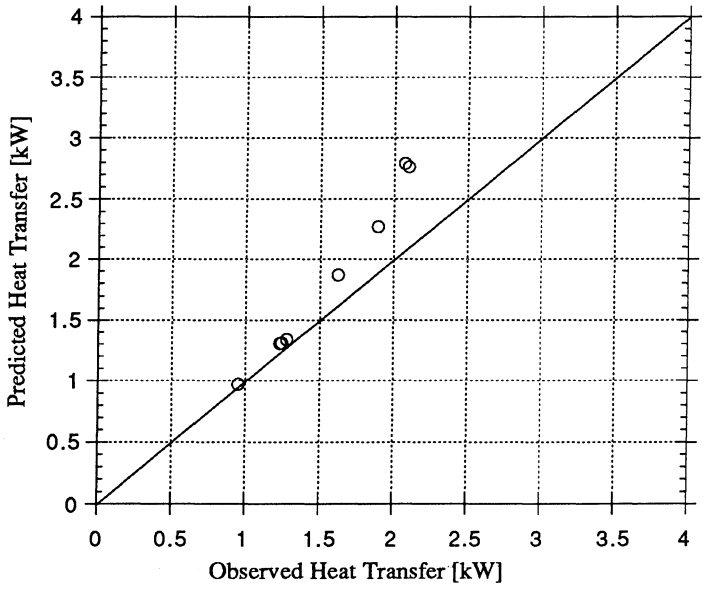

Figure 5.26: Heat Transfer for condensing R-22 flowing through a sqaure-port microchannel tube.

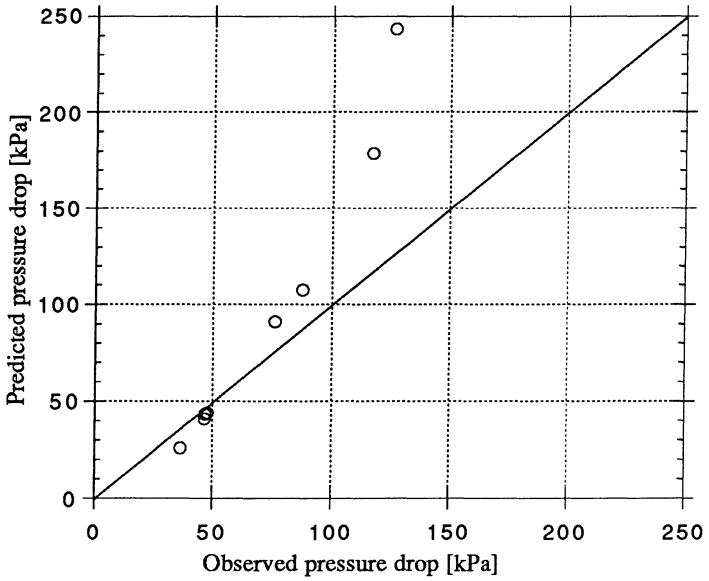

Figure 5.27: Pressure drop for condensing R-22 flowing through a square-port microchannel tube.

corresponding change in the total heat transfer is 1.5 %. This implies that errors in the prediction of the refrigerant-side heat transfer coefficient are reduced when the predicted total heat transfer is compared to the experimentally measured heat transfer.

5.5 Profile plots along the length of the microchannel tube

Figures 5.28, 5.29 and 5.30 show the profiles for temperature, pressure and quality along the microchannel tube as predicted by the model. These profiles are for R-134a condensing in a circular-port microchannel tube. It is interesting to observe the changes in the profiles where condensation begins and ends. The temperature at points where experimental values were available are also shown for comparision. The refrigerant temperature initially falls rapidly as the vapor gets cooled. Once condensation starts, the drop in temperature is dictated by the fall in pressure. After complete condensation,

the temperature again begins to fall rapidly as subcooled liquid loses sensible heat. The water temperature rises more uniformly except near the two ends where the curve is flatter because only sensible heat is being transferred. The temperature of water at the midpoint matches closely with the experimentally measured value.

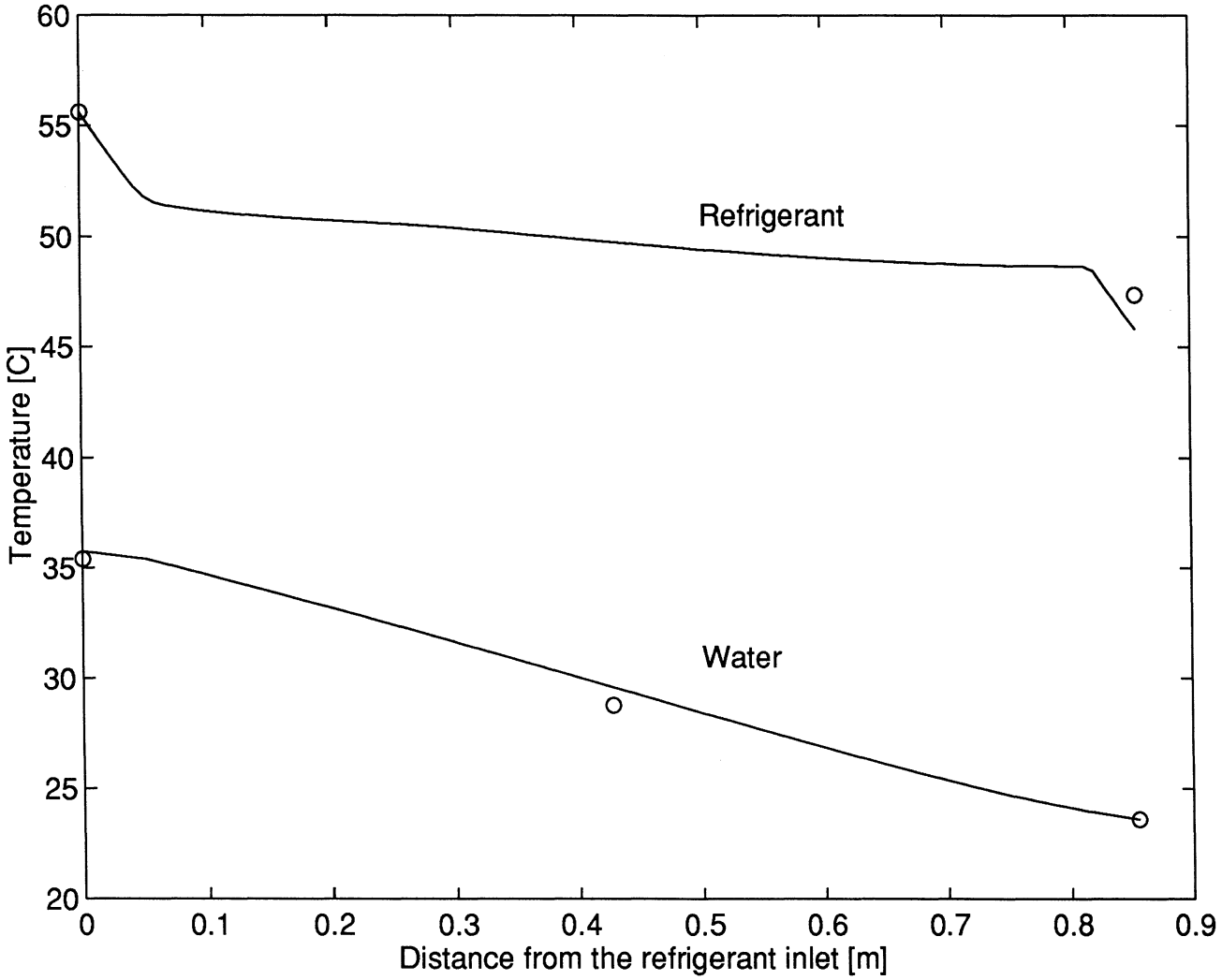

Figure 5.28: Predicted temperature profile along the microchannel tube. Circles denote experimentally measured values

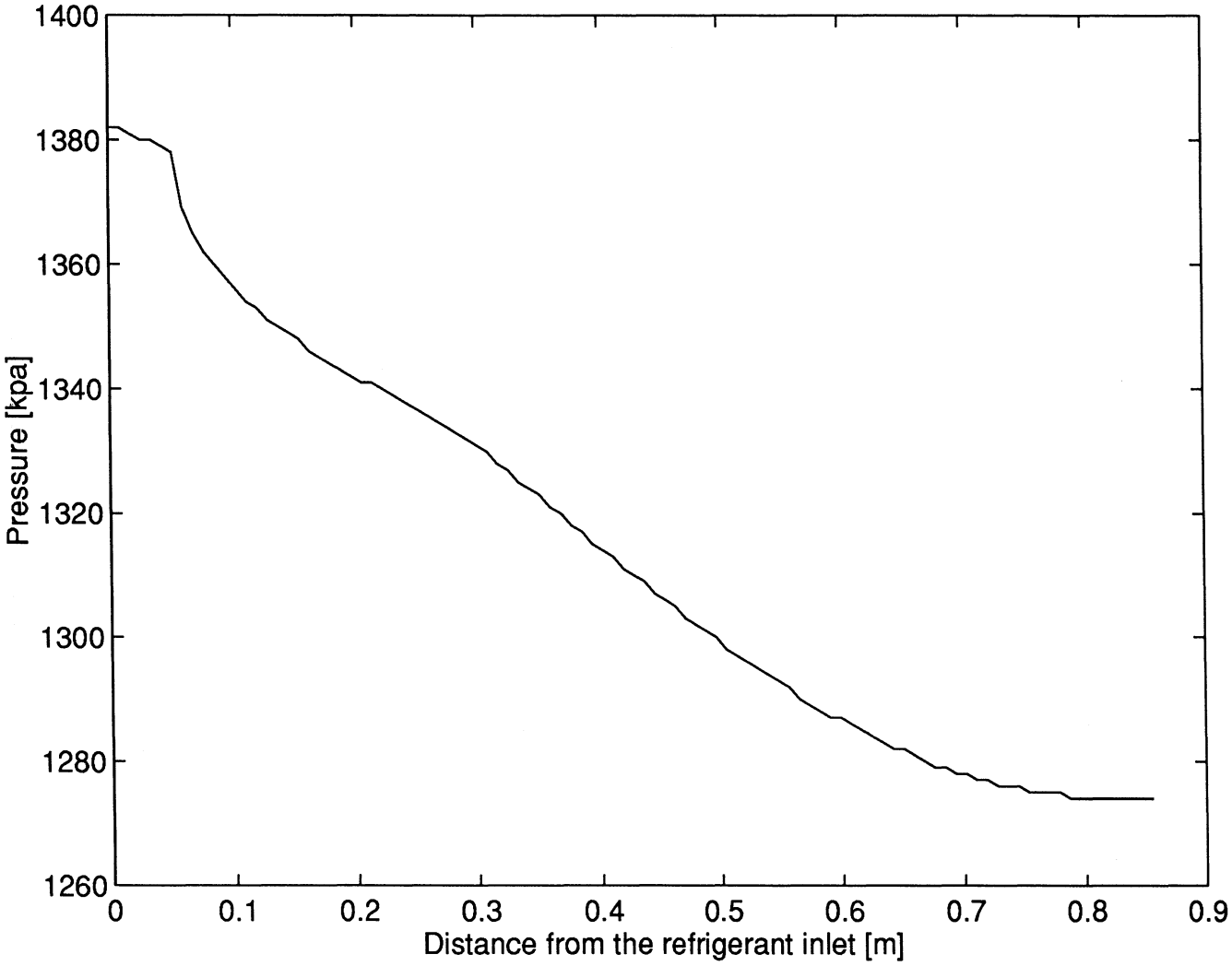

Figure 5.29: Predicted pressure profile along the microchannel tube.

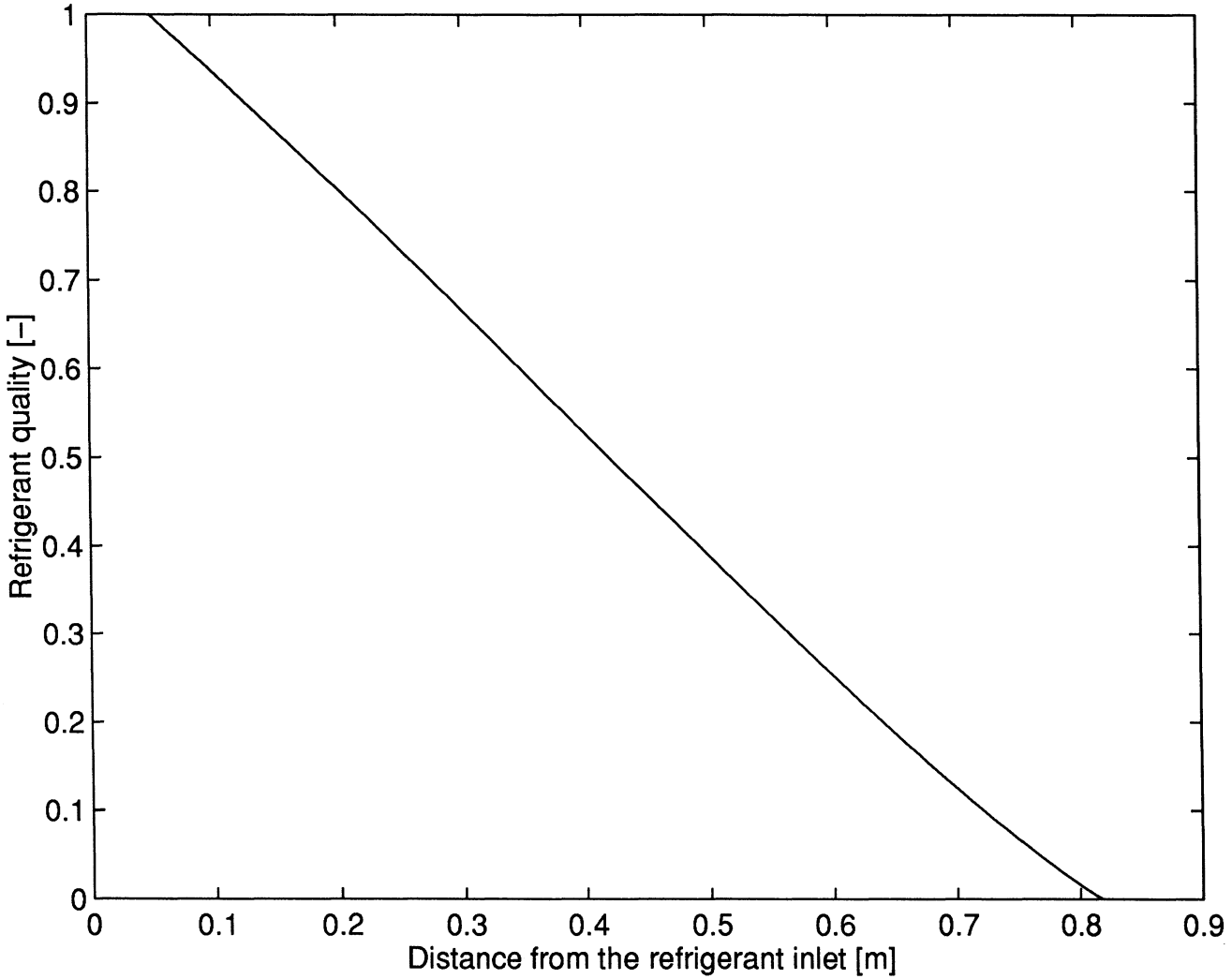

Figure 5.30: Predicted quality along the microchannel tube.

Chapter 6

Summary and Conclusions

In this study, the heat transfer and pressure drop characteristics for single-phase and two-phase flow of refrigerants in microchannel tubes was investigated. An experimental facility was developed which uses water flowing in counterflow as the heat sink fluid. Experimental data were colleted for three different refrigerants: R-22, R-134a and R-407C. A program was written to model the heat transfer and pressure drop in the test section and existing single-phase and two-phase correlations were compared with experimental data.

6.1 Summary of Results

- For subcooled liquid flow, the heat transfer coefficient for R-407C was found to be greater than that for R-22 and R-134a.
- The heat transfer coefficient for R-22 was found to slightly lesser than the other two refrigerants for condensing flow.
- The experimentally measured pressure drop for superheated R-134a was found to be very high. This discrepancy could not be resolved.
- The heat transfer predicted by the model using existing single-phase and two-phase correlation is agrees well with experimental data for most cases.

- The total heat transfer in the test section was found not to be very sensitive to the refrigerant-side heat transfer coefficient.
- The pressure drop predicted by the model for condensing flow is higher than experimental values.
- The heat transfer predicted for water-water data agrees with experimental results.

6.2 Recommendations for future research

- More superheated vapor data should be collected. Extreme care has to be taken while taking superheated vapor data because of high experimental uncertainties.
- Methods should be devised to ensure that the heat exchanger effectiveness of the test section is not close to unity, otherwise there is high uncertainty in estimating the heat transfer coefficient from the total heat transfer.
- Tube geometries other than circular-port should be tested extensively.
- The effect of oil on heat transfer and pressure drop could be studied.

Appendix A

Computer program for modeling test section

This appendix contains the FORTRAN program used in modeling the microchannel tube.

```
      program PressUA
c
c     Predict the heat transfer and pressure drop for single-phase and
c     two-phase heat transfer and pressure drop in a microchannel tube
c     with water flowing in counterflow.
c
c     started July,1997
c     by Abhay Vardhan
c     Univeristy of Illinois
c
c     INPUTS:
c     rowname: The name of the row being analysed
c     irefname: The number of the regrigerant. Follows REFPROP 5.0
c       conventions except for mixtures like R-407C where the number is
c       just 407.
c     m1: mass flow rate of refrigerant [kg/s]
c     m2: mass flow rate of water [kg/s]
c     T11: temperature at refrigerant inlet [C]
c     T2n: temperature at water inlet [C]
c     Pin: pressure at refrigerant inlet [kPa]
c     Dh: hydraulic diameter of the tube [m]
c     Deqs: nondimensional equivalent diameter (Deq/Dh) [-]
```

```
c     L: length of the heat exchanger part of the test section [m]
c     Kntf: Entrance loss coefficient in the transition piece[-]
c     Kexit: Exit loss coefficient in the transition piece[-]
c     Np: number of ports in the microchannel tube
c     itube: Tube type (1:circular, 2:square, 3: triangular)
c     SfoS: ratio of web surface area to total surface area for
c       inside fins
c     kt: thermal conductivity of tube material [kW/mK]
c     tfin: thickness of inside fins [m]
c     Lfin: length of inside fins [m]
c     UAoutside: Outside heat transfer coefficient times outside area
c       [kW/K]
c     Q1expt: Experimental heat transfer on the water side [kW]
c     Q2expt: Experimental heat transfer on the refirgerant side [kW]
c     Pdropexpt: Experimental pressure drop [kPa]
c
c     OUTPUTS:
c     rowname,irefname,Q1expt,Q2expt,Pdropexpt as in INPUTS
c     Fineff: the efficiency of inside fins
c     HXeff: effectiveness of the heat exchanger
c     Qpred: Predicted heat transfer [kW]
c     Pdrop: Predicted pressure drop [kPa]
c



      write(11,1002)'rowname','irefname','Reynolds no','Prandtl no',
     $     'Nusselt no','Darcy f','Fineff','HX eff'
     $     ,'Q1expt','Q2expt','Qpred','Pdropexpt','Pdrop'
 1    read (10,*,end=99) rowname,irefname,m1,m2,T11,T2n,Pin,Dh,Deqs,L
     $     ,Kntf,Kexit,Np,itube,SfoS,kt,tfin,Lfin,UAoutside,Q1expt
     $     ,Q2expt,Pdropexpt

      implicit none
      include 'common.h'

      double precision fd,L, m1, m2, T11, T2n,Dh,Across
      double precision UA,Q,Qpred,dx
      double precision P1,PexitLoss
      double precision CheckConverg,converg
c     P1 is the pressure at the inlet of the test section
      double precision tolr,pi
      parameter(tolr=1d-4,pi=3.141592654d0)
      integer i,j,MAXITER
```

```
      parameter(MAXITER=25)

      double precision Deqs,Kntf,UAoutside,UAinside
      integer Np,itube,irefname
      double precision vpt,mupt,cppt,kpt,FindFd,Nu,HXeff
      double precision Re,kPatoPa,specvol,Pcross,cpin,amu,k,Pr
      double precision En2n,En11,hwat,hpt,Kexit,Q1expt,Q2expt
     $     ,Pdropexpt,Twat
      double precision Pin
      parameter (kPatoPa = 1.d3)
      character*8 comment
      character*20 rowname
      double precision Rref,HTCin,Sref,SfoS,kt,tfin,Lfin,FinEff,Nuss
      double precision checkconverg2

      character*50 argv(6)
      integer iarg, iargc, marg


c     get command line arguments
      marg = iargc()
      if(marg.lt.2)stop 'usage: PressUA infile outfile [P En1 En2 x]'
      do iarg = 1, marg
         call getarg ( iarg, argv(iarg) )
      end do


c...  read input values
c
      open(unit=10,file=argv(1))
      open(unit=11,file=argv(2))
      if(marg.eq.6)then
         open(unit=12,file=argv(3))
         open(unit=13,file=argv(4))
         open(unit=14,file=argv(5))
         open(unit=15,file=argv(6))
      endif
      read(10,*)comment
      write(11,1002)'rowname','irefname','Reynolds no','Prandtl no',
     $     'Nusselt no','Darcy f','Fineff','HX eff'
     $     ,'Q1expt','Q2expt','Qpred','Pdropexpt','Pdrop'
 1    read (10,*,end=99) rowname,irefname,m1,m2,T11,T2n,Pin,Dh,Deqs,L
     $     ,Kntf,Kexit,Np,itube,SfoS,kt,tfin,Lfin,UAoutside,Q1expt
```

```
     $     ,Q2expt,Pdropexpt

c     initialize refrigerant properties
      if(irefname.eq.18)then
         call propSetActual(irefname,1,1)
      else
         call propSetActual(irefname,1,0)
      endif
c     account for the pressure drop in the Transition piece
      specVol = vpt(Pin,T11)
      Across = pi*Np*(Deqs*Dh)**2/4.d0
      Pcross = 4.d0*Across/Dh
      Sref = L*Pcross
      P1 = Pin -Kntf*0.5d0*(m1/Across)**2*specVol/kPatoPa
      En(1,1) = hpt(P1,T11)
      En(2,NODES) = hwat(T2n)

      write(*,*)'#######################################################'
      write(*,*)'Now processing rowname ',rowname

      dx=L/NCELLS


      call InitializeP(P1,Pdropexpt)
      call InitializeEn(m1,m2,Q1expt)

      i = 1
10    write(*,*)'*********************************************'
      Write(*,*)'Iteration:',i

      call PropertyValues
      call SaveValues
      j=1
20    write(*,*)'Sub iteration',j
      call UpdateP(m1,Across,Dh,dx,itube)
      Qpred=Q(UAoutside,m1,m2,T11,T2n,Sref,SfoS,kt,tfin,Lfin,Fineff,m1
     $     /Across,Dh)
      specVol = vol(NODES)
      PexitLoss =Kexit*0.5d0*(m1/Across)**2*specVol/kPatoPa
      converg=CheckConverg()
      write(*,*)'Convergence ',converg,' Qpred ',Qpred,' Pdrop ',Pin
     $     -P(Nodes)+PexitLoss
      j=j+1
```

```
c      if((converg.gt.tolr*10.d0).and.(j.lt.MAXITER))goto 20
       if(j.ge.MAXITER)then
          write(*,*)'Sub iterations not converging'
          goto 1
       endif
       converg=CheckConverg2()
       write(*,*)'Outer Convergence ',converg
       i=i+1
       if((converg.gt.tolr).and.(i.lt.MAXITER))goto 10
       if(i.ge.MAXITER)then
          write(*,*)'Outer iterations not converging'
          goto 1
       endif

       if(marg.eq.6)then
          write(12,1003)(P(i),i=1,NODES)
          write(13,1003)(T(i),i=1,NODES)
          write(14,1003)(Twat(En(2,i)),i=1,NODES)
          write(15,1003)(x(i),i=1,NODES)
       endif

       write(11,1001) rowname,irefname,Re,Pr,Nuss,fd,Fineff,HXeff,
     $      Q1expt,Q2expt
     $      ,Qpred,Pdropexpt,Pin-P(Nodes)+PexitLoss
1001   format(1x,A20," ",I4,100(" ",G12.4))
1002   format(1x,100(A15," "))
1003   format(1x,200(G12.4," "))
       goto 1
99     stop
       end


       subroutine updateP(m,Across,Dh,dx,tubetype)
       implicit none
       include 'common.h'
       integer tubetype
       double precision m,Across,fd,Dh,dx,G
       double precision vol1,vol2,kPatoPa
       double precision alphain,alphaout,dpacc,xmid,mufmid,kfmid,cpfmid
     $      ,volmid,rel,prl,kfmid,fdl,ftp,dpl
       parameter(kPatoPa=1000.d0)
       integer i
       double precision findfd,findftp
```

```
      double precision mumid,re

c     save the old values of P
      do i=1,NODES
         Pold(i)=P(i)
      enddo
      G = m/Across
      do i=2,NODES
         if((x(i-1).gt.0.d0).and.(x(i-1).lt.1.d0)
     $        .and.(x(i).gt.0.d0).and.(x(i).lt.1.d0))then
c     two-phase conditions throughout the cell
            alphaIn=x(i-1)*volg(i-1)/((1.d0-x(i-1))*volf(i-1)+x(i-1)
     $           *volg(i-1))
            alphaOut=x(i)*volg(i)/((1.d0-x(i))*volf(i)+x(i)*volg(i))
c     acceleration pressure drop
            dpAcc=G**2*(x(i)**2*volg(i)/alphaOut+
     $           (1.d0-x(i))**2*volf(i)/(1.d0-alphaOut)
     $           -x(i-1)**2*volg(i-1)/alphaIn-
     $           (1.d0-x(i-1))**2*volf(i-1)/(1.d0-alphaIn))
c     superficial liquid pressure drop
            xmid = (x(i)+x(i-1))/2.d0
            mufMid = (muf(i)+muf(i-1))/2.d0
            kfMid = (kf(i)+kf(i-1))/2.d0
            CpfMid = (Cpf(i)+Cpf(i-1))/2.d0
            volMid = (volf(i)+volf(i-1))/2.d0
            Rel=G*(1.d0-xmid)*dh/mufMid
            Prl = cpfmid*1.d3*mufMid/kfMid ! cp is in kJ/kg
            fdl=findfd(Rel,tubetype)
            dpl=0.5d0*(G*(1.d0-xmid))**2*volmid*dx/Dh*fdl
            ftp = findftp((xtt(i)+xtt(i-1))*0.5d0)
            P(i)=P(i-1)-(dpAcc+dpl*ftp)/kPatoPa
         else
c     if one of the nodes is two-phase, assume the whole segment to be
c     single-phase with specific volume equal to the single phase node

c     estimate the Friction Factor (Darcy's)
            muMid = (muf(i)+muf(i-1))/2.d0
            Re=G*dh/muMid
            fd=FindFd(Re,tubetype)
            if((x(i-1).gt.0.d0).and.(x(i-1).lt.1.d0))then
               vol1 = vol(i)
            else
               vol1 = vol(i-1)
```

```
            endif
            if((x(i).gt.0.d0).and.(x(i).lt.1.d0))then
               vol2 = vol(i-1)
            else
               vol2 = vol(i)
            endif
            P(i) = P(i-1) -(0.5d0*G**2*0.5d0*(vol1+vol2)*dx/Dh*fd
     $           +G**2*(vol1-vol2))/kPatoPa
         endif
       enddo
c      print *,'Pressure',P
c      print *,'Old Pressure',Pold
       return
       end


       double precision function CheckConverg()
       implicit none
       include 'common.h'
       double precision converg,temp
       integer i

       converg = 0.d0
       do i=1,NODES
          temp = dabs((En(1,i)-EnOld(1,i))/En(1,i))
          if(temp.gt.converg)converg=temp
          temp = dabs((En(2,i)-EnOld(2,i))/En(2,i))
          if(temp.gt.converg)converg=temp
          temp = dabs((P(i)-POld(i))/P(i))
          if(temp.gt.converg)converg=temp
       enddo

       CheckConverg=converg

       return
       end


       subroutine Savevalues()
       implicit none
       include 'common.h'
       integer i
       do i=1,NODES
```

```
         Pold2(i)=P(i)
         EnOld2(1,i)=En(1,i)
         EnOld2(2,i)=En(2,i)
      enddo
      return
      end

      double precision function CheckConverg2()
      implicit none
      include 'common.h'
      double precision converg,temp
      integer i

      converg = 0.d0
      do i=1,NODES
         temp = dabs((En(1,i)-EnOld2(1,i))/En(1,i))
         if(temp.gt.converg)converg=temp
         temp = dabs((En(2,i)-EnOld2(2,i))/En(2,i))
         if(temp.gt.converg)converg=temp
         temp = dabs((P(i)-POld2(i))/P(i))
         if(temp.gt.converg)converg=temp
      enddo

      CheckConverg2=converg

      return
      end




      subroutine InitializeP(P1,Pdropexpt)
      implicit none
      include 'common.h'
      double precision P1,Pdropexpt
      integer i

c      G = m1/Across
c     The following code raises IEEE floating point exceptions Why?
c      pdrop = 0.5d0*vph(P1,En11)*G**2*L/(Dh*kPatoPa)*fd
c     Interpolate the rest
      do i = 1,NODES
         P(i)=P1-pdropexpt/NCELLS*(i-1.d0)
```

```
      enddo

      return
      end



      subroutine InitializeEn(m1,m2,Qtot)
      implicit none
      include 'common.h'
      double precision Qtot,m1,m2
      integer i

      En(1,NODES) = -Qtot/m1+En(1,1)
      En(2,1) = En(2,NODES)+Qtot/m2

c     Interpolate the rest of the Enthalpy values
      do i = 1,NODES
         En(1,i)=En(1,1)+(En(1,NODES)-En(1,1))/NCELLS*(i-1.d0)
         En(2,i)=En(2,1)+(En(2,NODES)-En(2,1))/NCELLS*(i-1.d0)
      enddo

      return
      end



      double precision function Q(UAoutside,m1,m2,T11,T2n,Sref,SfoS,kt
     $     ,tfin,Lfin,Fineff,G,Dh)
c     function to find the error between the experimental Q and the one
c     predicted by UA

      implicit none
      include 'common.h'
      double precision Qpred1,Qpred2,Qpred
      double precision Sref,SfoS,kt,tfin,Lfin,Fineff,G,Dh

      double precision m1,m2
      integer i

      double precision UAoutside
      double precision T11,T2n
```

```
c     update the old values
      do i = 1, NODES
         EnOld(1,i) = En(1,i)
         EnOld(2,i) = En(2,i)
      enddo

c     formulate the coeffiecients
      call coeff(UAoutside,m1,m2,Sref,SfoS,kt,tfin,Lfin,Fineff,G,Dh)

c     solve the equations
      call cfhxs (a, b, c, d, En, y, NODES, En(1,1), En(2,NODES), work)

c     print *, (T1(En(1,i)), i = 1, NODES)
c     print *, (T2(En(2,i)), i = 1, NODES)
c     print *, (T1(EnOld(1,i)), i = 1, NODES)
c     print *, (T2(EnOld(2,i)), i = 1, NODES)

      Qpred1 = m1*(En(1,1)-En(1,NODES))
      Qpred2 = m2*(En(2,1)-En(2,NODES))
      Qpred = 0.5d0*(Qpred1+Qpred2)
c     write(*,*)'Qpred1 ',Qpred1,' Qpred2 ',Qpred2,' Qpred ',Qpred
      Q=Qpred
      return
      end

      subroutine coeff(UAoutside,m1,m2,Sref,SfoS,kt,tfin,Lfin,Fineff,G
     $     ,dh)
      implicit none
      include 'common.h'
      integer i
      double precision UAoutside,m1,m2
      double precision temp1,temp2,temp3,temp4,temp5
      double precision cpwat,twat
      double precision UAcell,HTCin,Sref,SfoS,kt,tfin,Lfin,Fineff
     $     ,UAinside
      double precision Sref,SfoS,kt,tfin,Lfin,Fineff
      double precision  twophasehtc,singlephasehtc,rref
      double precision xmid,mufmid,kfmid,cpfmid,volfmid,Xttmid,mumid
     $     ,kmid,cpmid
      double precision G,dh

      do  i = 1, NCELLS
```

```
          if((x(i).gt.0).and.(x(i).lt.1).and.(x(i+1).gt.0)
     $         .and.(x(i+1).lt.1))then
            xmid = (x(i)+x(i+1))/2.d0
            mufmid = (muf(i)+muf(i+1))/2.d0
            kfmid = (kf(i)+kf(i+1))/2.d0
            Cpfmid = (Cpf(i)+Cpf(i+1))/2.d0
            volfmid = (volf(i)+volf(i+1))/2.d0
            xttmid = (xtt(i)+xtt(i+1))/2.d0

            HTCin=TwoPhaseHTC(xmid,mufmid,kfmid,cpfmid,volfmid,Xttmid,G
     $           ,Dh)
          else
c     if one of the nodes is two-phase consider the whole segment as
c     single-phase and take the properties at the single-phase node
            if((x(i).gt.0).and.(x(i).lt.1))then
               mumid = muf(i+1)
               kmid =  kf(i+1)
               Cpmid = Cpf(i+1)
            else if((x(i+1).gt.0).and.(x(i+1).lt.1))then
               mumid = muf(i)
               kmid =  kf(i)
               Cpmid = Cpf(i)
            else
c     for single phase transport properties are stored in muf,kf,etc
               mumid = (muf(i)+muf(i+1))/2.d0
               kmid = (kf(i)+kf(i+1))/2.d0
               Cpmid = (Cpf(i)+Cpf(i+1))/2.d0
            endif
            HTCin=SinglePhaseHTC(mumid,cpmid,kmid,G,dh)
          endif

          HTCin=HTCin/1.d3  !HTCin has to be in [kW/m^2-K]

c     estimate the UAinside
          UAinside=1.d0/Rref(HTCin,Sref/NCELLS,SfoS,kt,tfin,Lfin,Fineff)
          UAcell = UAinside*UAoutside/NCELLS/(UAinside+UAoutside/NCELLS)


          temp1=UAcell/2.d0/m1*cpInv(i)
          temp2=UAcell/2.d0/m1*cpInv(i+1)
          temp3=UAcell/2.d0/m1/Cpwat(EnOld(2,i))
          temp4=UAcell/2.d0/m1/Cpwat(EnOld(2,i+1))
          temp5=(Twat(EnOld(2,i))+Twat(EnOld(2,i+1))
```

```
$        -T(i)-T(i+1))
     a(1,i) = 1.d0 - temp1
     b(1,i) = -1.d0 - temp2
     c(1,i) = temp3
     d(1,i) = temp4
     y(1,i) = -UAcell/2.d0/m1*temp5
$         -temp1*EnOld(1,i)-temp2*EnOld(1,i+1)+temp3*EnOld(2,i)
$         +temp4*EnOld(2,i+1)
     temp1=temp1*m1/m2
     temp2=temp2*m1/m2
     temp3=temp3*m1/m2
     temp4=temp4*m1/m2
     a(2,i) = -1.d0-temp3
     b(2,i) = 1.d0-temp4
     c(2,i) = temp1
     d(2,i) = temp2
     y(2,i) = UAcell/2.d0/m2*temp5
$         +temp1*EnOld(1,i)+temp2*EnOld(1,i+1)-temp3*EnOld(2,i)
$         -temp4*EnOld(2,i+1)
 enddo
 return
 end



C     ****************************************************************
c     This function borrowed from Matt Heun's code (Heun(1995))

      double precision function Rref(href,Sref,SfoS,k,tfin,Lfin,eta0)

      implicit none
      double precision Rref,href,Sref,SfoS,k,tfin,Lfin

C     This function returns refrigerant-side resistance for
C     project 25/48 tubes given heat transfer coefficient,
C     thermal conductivity, and other geometric variables.

C     Inputs:

C     href = refrigerant-side heat transfer coefficient [kW/m^2-K]
C     Sref = total refrigerant-side surface area [m^2]
C     SfoS = Sfin/Sref = ratio of fin surface area to total Surf Area
C     k = fin thermal conductivity [kW/m-K]
```

```
C     tfin = fin thickness [m]
C     Lfin = fin length [m]

C     Outputs:

C     Rref = refrigerant-side thermal resistance [K/kW]

      double precision mL,etaf,eta0

C     Webs considered as fins.
C     Normally the fin parameter, m is given as
C     m = sqrt(hP/(kAc)) where P is the fin perimeter
C     and Ac is the fin cross section.  However, for the
C     case of project 25/48, we can use
C     P/Ac = (2w) / (wt) = 2/t, and
C     m = sqrt(2h/(kt))

      mL = Lfin*dsqrt(2.0d0*href/(k*tfin)) !fin parameter m*L
      etaf = tanh(mL) / mL      !web fin efficiency

C     Surface efficiency
      eta0 = 1.0d0 - SfoS*(1.0d0-etaf)

C     Refrigerant-side resistance
      Rref = 1.0d0 / (href*Sref*eta0)
      return
      end


      subroutine PropertyValues
      implicit none
      include 'common.h'
      integer i
      double precision Ts,Enf,Eng,Sf,Sg,hfg
      double precision kph,muph
      do i=1,NODES
         call Property(En(1,i),P(i),T(i),x(i),vol(i),Cpf(i),Cpinv(i)
     $        ,muf(i),kf(i),volg(i),Cpg(i),mug(i),kg(i),volf(i),Cpf(i)
     $        ,muf(i),kf(i))
         if((x(i).gt.0).and.(x(i).lt.1))then
            xtt(i)=(volf(i)/volg(i))**0.5*(muf(i)/mug(i))**0.1*
     $           ((1.d0-x(i))/x(i))**0.9
            CpInv(i)=0.d0
```

```
   endif
enddo
return
end
```

List of References

Akers, W. W. and Rosson, H. F. (1960). Condensation inside a horizontal tube. *Chemical Engineering Progress Symposium Series*, 56(30):145–149.

Bhatti, M. S. and Shah, R. K. (1987). *Turbulent and Transition Flow Convective Heat Transfer in Ducts In S. Kakac, R. K. Shah, and W. Aung (Eds.), Handbook of Single-phase Convective Heat Transfer.* John Wiley and Sons.

Carey, V. P. (1992). *Liquid-vapor Phase Change Phenomena.* Hemisphere, New York.

Chisholm, D. and Laird, A. D. K. (1958). Two-phase flow in rough tubes. *In Transactions of the American Society of Mechanical Engineers. San Francisco,CA*, 80:276–286.

Churchill, S. W. (1977). Friction-factor equations spans all fluid-flow regimes. *Chemical Engineering*, pages 91–92.

Dobson, M. K. (1994). *Heat Transfer and Flow Regimes During Condensation in Horizontal Tubes.* PhD thesis, University of Illinois.

Gerhart, P. M. and Gross, R. J. (1985). *Fundamentals of Fluid Mechanics.* Addison-Wesley Publishing Company, Reading, Massachusetts.

Gnielinski, V. (1976). New equations for heat and mass transfer in turbulent pipe and channel flow. *International Chemical Engineering*, 16(2):359–368.

Goodremote, C. E., G. L. A. and Costello, N. F. (1988). Compact air cooled air conditioning condenser (SAE technical paper series no. 880445). *The Engineering Society for Advancing Mobility in Land, Sea, Air and Space.*

Graham, T. P. (1995). Friction and heat transfer characteristics for single-phase flow in microchannel condenser tubes. Master's thesis, University of Illinois at Urbana-Champaign.

Guntly, L. (1990). Use of HCFC-22 in a vehicular air conditioning system (SAE technical paper series no. 900599). *The Engineering Society for Advancing Mobility in Land, Sea, Air and Space.*

Heun, M. K. (1995). *Performance and Optimization of Microchannel Condensers.* PhD thesis, University of Illinois at Urbana-Champaign.

Incropera, F. P. and Dewitt, D. P. (1990). *Fundamental of Heat and Mass Transfer.* John Wiley & Sons, New York.

Jones, O. C. (1976). An improvement in the calculation of turbulent friction in rectangulr ducts. *Journal of Fluids Engineering*, pages 173–181.

Lockhart, R. W. and Martinelli, R. C. (1949). Proposed correlation of data for isothermal two-pase, two-component flow in pipes. *Chemical Engineering Progress*, 45(1):39–48.

Meyer, J. J. (1996). *Heat transfer coefficients in enhanced tubing for R502 and R22 alternatives and Capillary tube flow for R22 and alternatives.* PhD thesis, University of Illinois at Urbana-Champaign.

Mikic, B. B., Vujisic, L. B., and Kapat, J. (1994). Turbulent transition and maintenance of turbulence; implication to heat transfer augmentation. *International Journal of Heat and Mass Transfer*, 37,Suppl. 1:425–431.

Moffat, R. J. (1988). *Describing the Uncertainties in Experimental Results*, volume 1.

Moody, L. F. (1944). Friction factors for pipe flow. *Transactions of the American Society of Mechanical Engineers*, pages 671–684.

Obot, N. T. (1988). Determination of incompressible flow friction in smooth circular and noncircular passages: A generalized approach including validation of the nearly century old hydraulic diameter concept. *Journal of Fluids Engineering*, 110:431–440.

Palen, J. W., K. R. S. and Yang, Z. F. (1993). What we still don't know about condensation in tubes. in condensation and condenser design. *American Society of Mechanical Engineers*, pages 19–53.

Shah, M. M. (1979). A general correlation for heat transfer during film condensation inside pipes. *International Journal of Heat and Mass Transfer*, 22:547–556.

Shah, R. K. and London, A. L. (1978). *Laminar Flow Forced Convection in Ducts.* Academic Press, New York.

Struss, R. A. and Gabbey, L. W. (1990). Performance comparison of HFC-134a and CFC-12 in a heavy truck air conditioning system (SAE techmical paper series no. 902261). *The Engineering Society for Advancing Mobility in Land, Sea, Air, and Space.*

Struss, R. A., Henkes, J. P., El-Bourini, M. R., and Eigenberger, J. J. (1989). Refrigerant charge reduction through the application of a new vehicular condenser (SAE technical paper series no. 890226). *The Engineering Society for Advancing Mobility in Land, Sea, Air and Space.*

Struss, R. A., Henkins, J. P., and Gabbey, L. W. (1990). Performance comparison of HFC-134a and CFC-12 with various heat exchangers in automotive air conditioning systems (SAE technical paper series no. 900598). *The Engineering Society for Advancing Mobility in Land, Sea, Air, and Space.*

Sugihara, A. and Lukas, H. G. (1990). Performance of parallel flow condensers in vehicular applications (SAE technical report no. 900597). *The Engineering Society for Advancing Mobility in Land, Sea, Air, and Space.*

Tait, R. D., Rogers, C. J., Cottone, A. J., Henkes, J. P., and Saperstein, Z. P. (1991). Corrosion resistance of the as brazed pf heat exchanger as achieved by alloy selection (SAE technical paper series no. 910594). *The Engineering Resource for Advancing Mobility.*

Vij, A. K. (1996). Modeling of two-phase flows in horizontal tubes. Master's thesis, University of Illinois at Urbana-Champaign.

Webb, R. L. and Yang, C. Y. (1995). A comparison of R-12 and R-134a condensation inside small extruded aluminium plain and micro-fin tubes. In *In 1995 Vehicle Thermal Management Systems Conference II*, pages 77–85. Mechanical Engineering Publication, London.

Zietlow, D. C. (1995). *Heat Transfer and Flow Characteristics of Condensing Refrigerants in Small-channel Crossflow Heat Exchangers (ACRC TR-73).* PhD thesis, University of Illinois at Urbana-Champaign.